Chapter 5

Physico – Chemical Characteristics of Aerosol Generated by Burning of Bare and Alumina Coated Graphite

In the previous chapter, we discussed the physical characterization of graphite. The experimental procedure followed for aerosol generation were also explained. In the present chapter, characterization of aerosol produced by burning bare and alumina coated graphite under different test conditions has been presented. This chapter comprises of four section. In the first section, the size and size distribution of the aerosol produced by burning bare graphite at constant temperature has been presented (Heating protocol 1). The second section focuses on the characterization of aerosol produced by burning bare graphite at different heating rate (Heating protocol 2). The characterization of alumina coated graphite heated under constant temperature conditions is discussed in sections three. A comparative evaluation of the size characteristics of aerosol generated by bare and coated graphite is also presented. The last section discusses the proposed mechanism of aerosol formation during burning of bare and coated graphite.

5.1 Bare graphite burning at constant temperature

In the present section, the study investigates the graphite particle characterization under constant temperature heating conditions. The number concentration and the geometric mean diameter have been measured. The emission of CO and CO_2 gases during graphite burning has been reported in order to estimate the transition temperature (discussed in chapter 1). The surface characterization of the sample has been done using Scanning Electron Microscopy (SEM) to gain understanding about the change in surface morphology during oxidation.

5.1.1 Effect of heating on surface morphology during oxidation

The changes occurring on the surface of the graphite sample after heating and oxidation were studied using SEM. Figure 5.1a represent the SEM image of unburnt graphite sample used in experiments. The SEM images of the residual graphite samples after oxidation is presented in Figure 5.1b-f. As can be seen, the unburnt graphite surface reveals a flaky appearance (Figure 5.1a). It can be seen from Figure 5.1b-c, that as the test temperature is increased from 500 to 600 °C, the number of flakes on the surface increase. It was also observed that at 600 °C, cavities start to form on the surface. With further increase in temperature, the size of cavities gradually increased. However, beyond 700 °C, the surface appearance changed and number of flakes decreased (Figure 5.1d-f). At lower temperature (say less than 700 °C) the rate of reaction between the graphite and oxygen is slow as compared to that at higher temperature. Furthermore, the rate of diffusion of oxygen into the graphite is higher and it penetrates deep into the graphite block. In such a condition, the bulk of oxygen penetrates inside the block, leaving a small quantity available at the surface. As a result of thermal stress induced by internal fissure, cracks, structural imperfections and pores, the graphite surface transform into one with a flaky appearance. However, at higher temperatures (i.e., above 700 °C), the rate of reaction (chemical kinetics) is exponentially faster than oxygen penetration (Kane et al., 2013). Additionally, the depth of penetration of oxygen is limited to the sub-surface region. In such conditions, reaction takes place only at the outer surface. It causes the formation of a fused- type surface with large cavities on the surface and vanishing of the flaky structure.

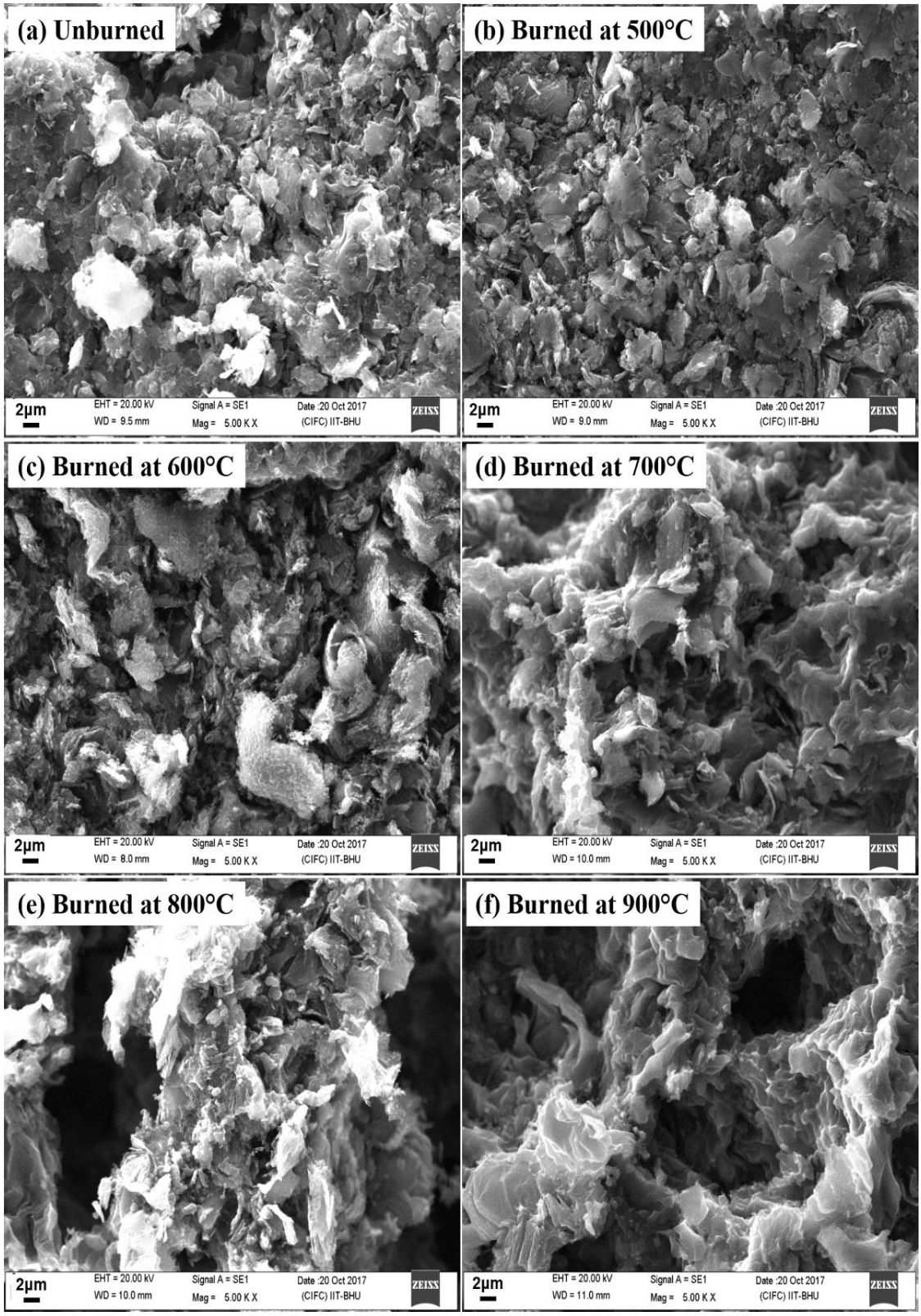

Figure 5.1: SEM analysis of residual samples after burning in air at constant temperatures for 2-hours

5.1.2 Characteristics of generated particles

The total number concentration of the aerosol particles generated due to the burning (oxidation) of graphite sample at a constant temperature (in the range of 500 - 900 °C) and a flowrate of 25 $Lmin^{-1}$ is depicted in Figure 5.2. For all investigated temperatures, the number concentration shows a decreasing trend of particle number concentration with time. At 500 °C, particle generation was not detected. However, particle number concentration increased considerably when the temperature was increased to 600 °C. The highest particle emission was observed at a temperature of 700 °C. With further increase in oxidation temperature beyond 700 °C, a reduction in particle concentration was observed. At 900 °C, the particle emission dropped significantly. A possible reason for this observation is linked to the activation energy of graphite oxidation, which becomes maximum at 700 °C and then starts decreasing (Kane et al., 2017). Activation energy is a direct measure of the thermodynamic energy barrier to a reaction. This implies that the maximum energy barrier to oxidation occurred at 700 °C which resulted in the generation of maximum incomplete combustion products. SEM images also point to a transition temperature of 700 °C for graphite surface, where flaky structure changes into the fused-type structure (Figure 5.1). Details on the mechanism of variation in particle generation rate with temperature are presented in a later section (section 5.4).

Figure 5.2 shows that at the beginning of sample insertion, the particle emission was relatively higher. However, as heating continued at constant temperature, the particle emission started to decline for all the cases. Prolonged heating results in the reduction of surface area of the sample and consequently deactivation of reaction sites (Kane et al., 2013; Radovic et al., 2011).

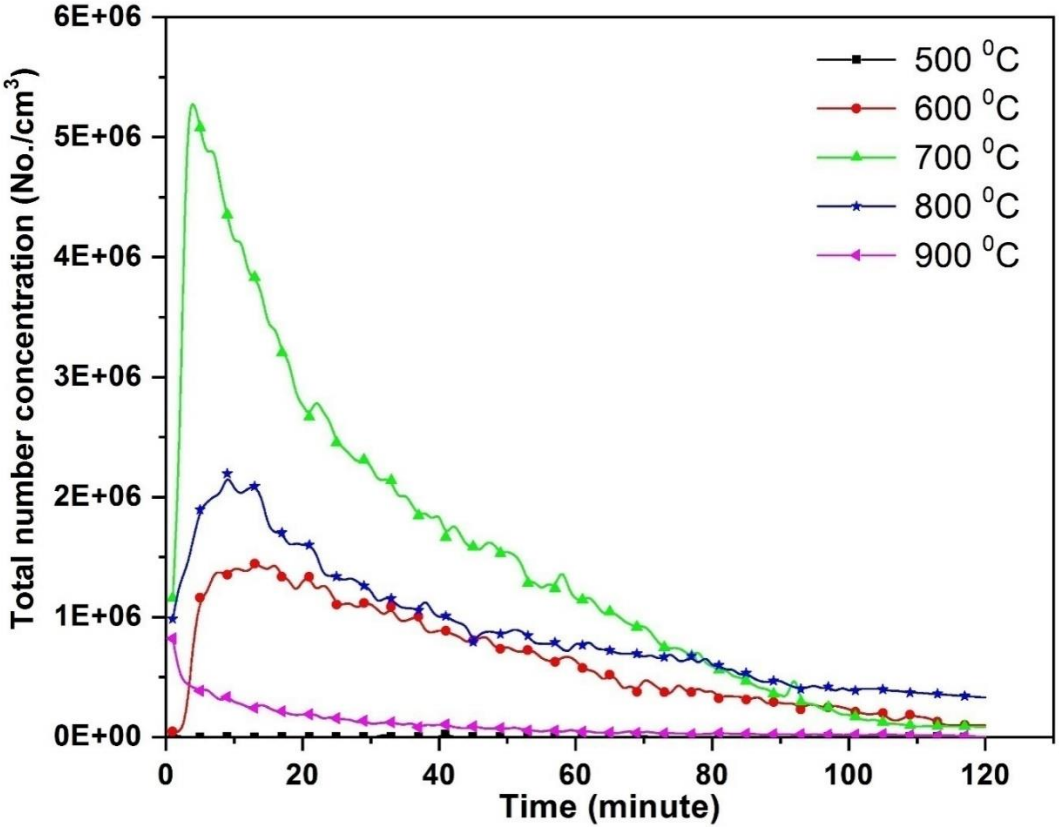

Figure 5.2: Particle number concentration at different temperatures for 2-hours combustion duration at 25 $Lmin^{-1}$

5.1.3 Size distribution

The dependence of the physical and chemical properties of a particle upon its size and distribution was discussed in chapter 1. In the present study, we analyse the size distribution of particles generated under various test conditions. Figure 5.3 depicts the average number concentration for different bin sizes at all test temperatures. The average particle number concentration was calculated for a 2-hours burning time period of the sample. It was found that at 500 °C, particles observed in different size bins were negligible (mostly in the background range). At 600 and 800 °C, most of the particles were in the small nucleation mode size range (10 - 15.4 nm). In contrast, particles in size range 10 - 50 nm (peak at around 15 nm) were observed for the case of burning at 700 °C. Presence of particles in small nucleation mode size ranges at 900 °C is probably due to modification (reduction) of size of particles due to reactions at particle surface by

diffusion limited mechanisms. Particles above 100 nm were observed for temperatures 600 - 800 °C. No significant concentration of particles was measured between ≈ 50 - 100 nm size range. The pathways of particle generation and the respective mechanisms have been explained in detail in section 5.4 of the present chapter.

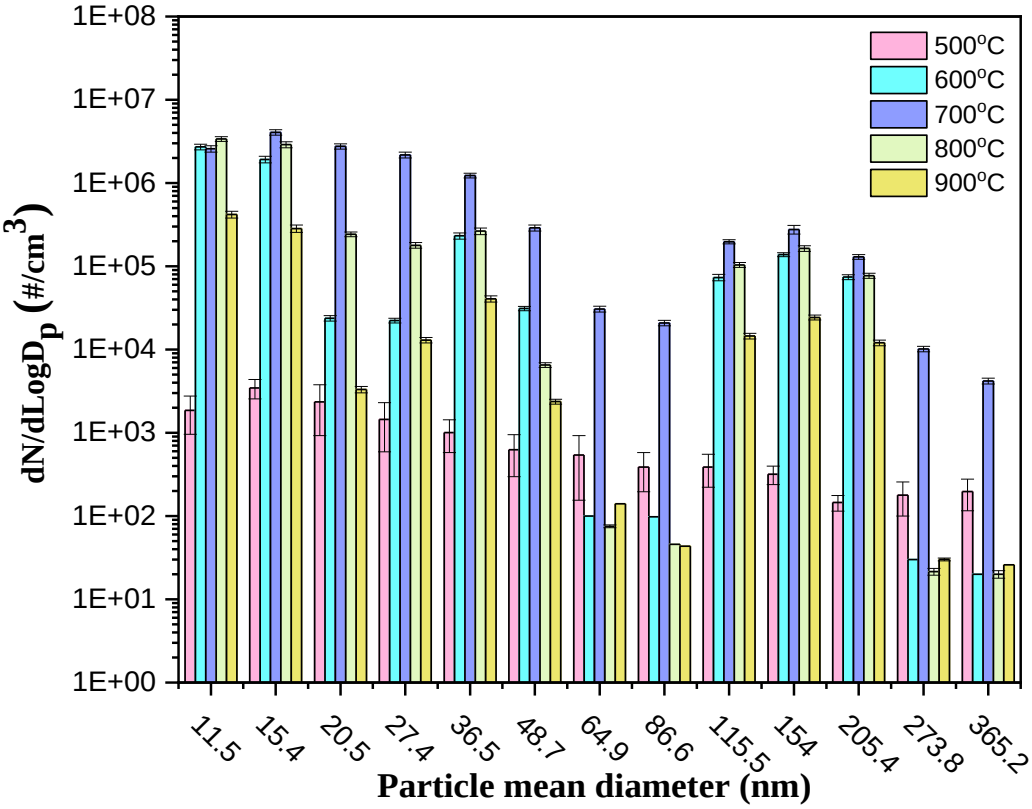

Figure 5.3: Particle size distribution after 2-hours of combustion

For understanding the effect of oxidation temperature on the burning characteristics, the mass concentration is an essential factor along with the particle count. The effect of burning temperature on the mass concentration has been shown in Figure 5.4. With the initiation of burning, the mass concentration was found to be highest at 700 °C. For all temperatures, the highest value of mass concentration was recorded for initial times when the sample started to burn in the furnace. As combustion proceeded, the mass concentration of emitted particles started to decrease. Figure 5.4 also depicts a sharp decrease in the particle mass concentration at 700 °C as compared to other temperatures.

The increase in mass concentration at 700 °C during 40 to 70 minutes can be attributed to an increase in larger sized particles during this time, as observed in Figure 5.5.

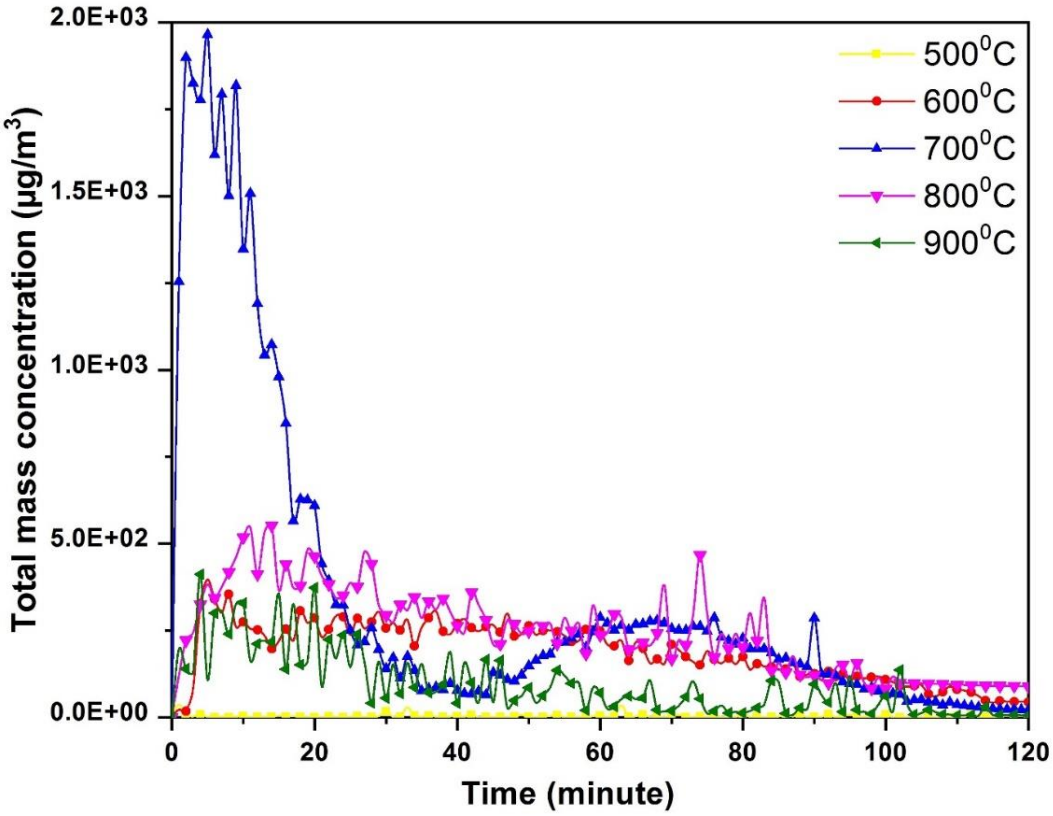

Figure 5.4: Particle mass concentrations at different temperatures

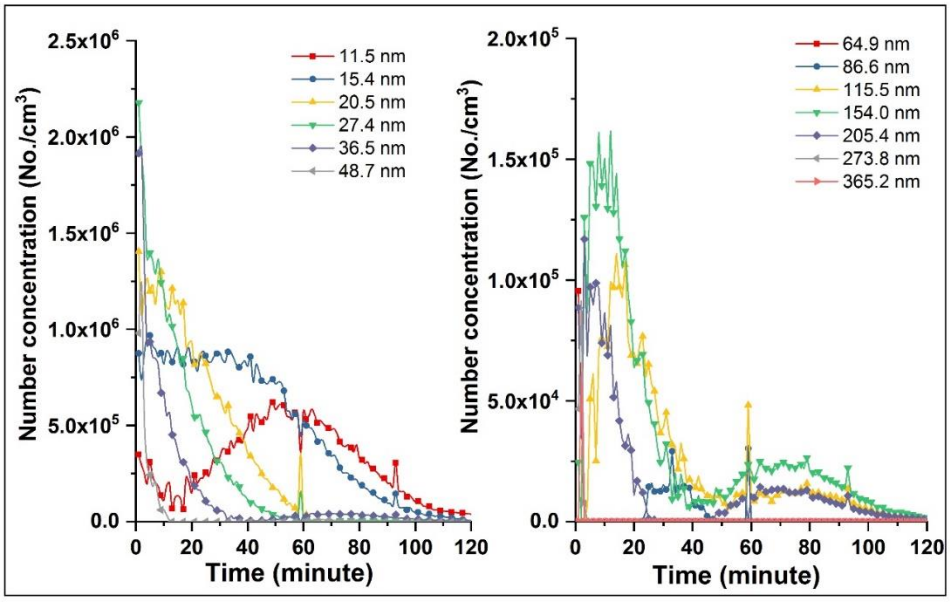

Figure 5.5: Time evolution of size segregated particles at 700 °C

5.1.4 Effect of carrier gas flow rate

The effect of flow rate on particle generation is studied in this section. The air flow rates were varied between 10 and 25 $Lmin^{-1}$ for this purpose (Figure 5.6). It was observed that the number concentration increases with increase of flow rate. For instance, at 700 °C, the peak value of number concentration for the case of 25 $Lmin^{-1}$ was found to be 5.34 x 10^6 #/cm^3 while it was 3.06 x 10^6 #/cm^3 for the case of 10 $Lmin^{-1}$. This observation is attributed to the effect of higher erosion at higher flow rates. The graphite surface becomes softer at higher temperatures. When air at higher flow rate impinges on soft surface, it would tend to detach the particles from the surface more effectively, resulting in larger number concentration.

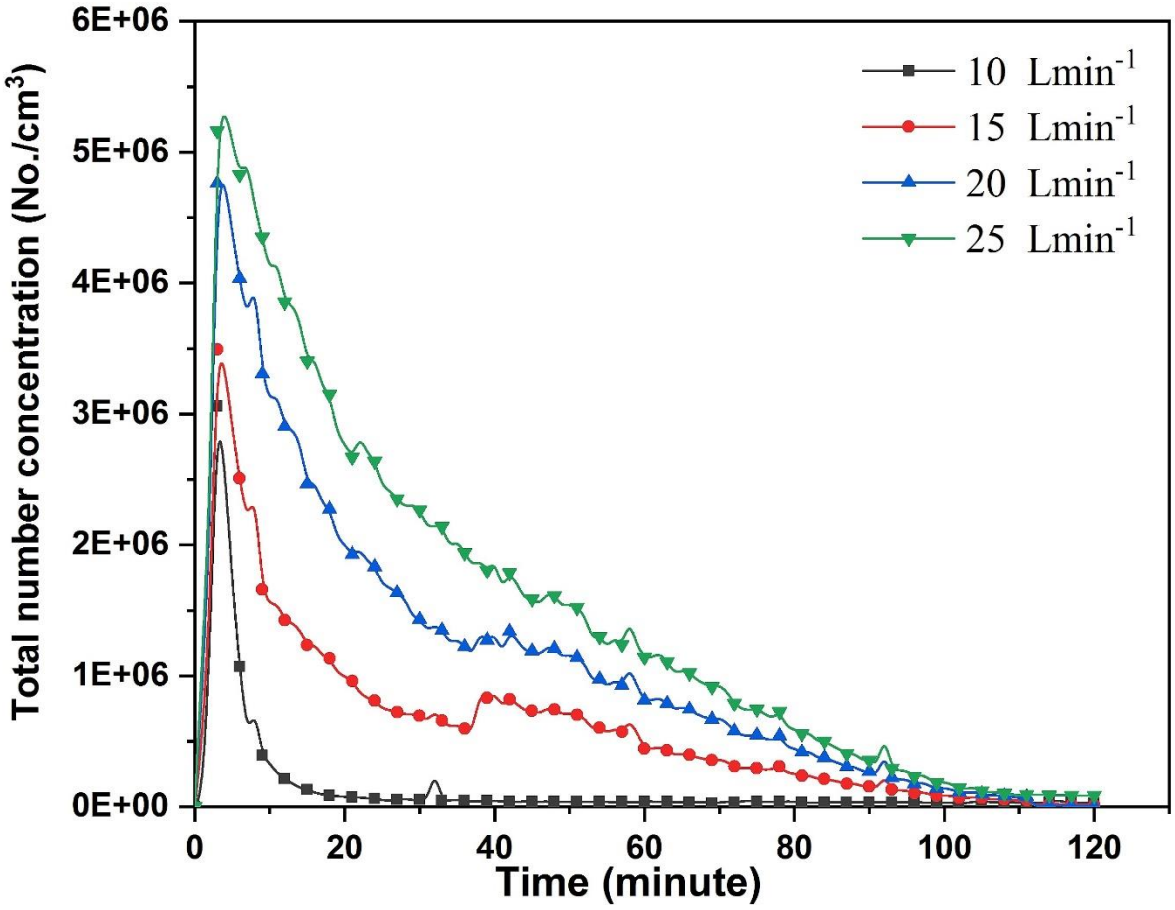

Figure 5.6: Particle number concentration at different flow rates for 2-hours combustion (burning temperature: 700 °C)

5.1.5 Gas analysis

The emission of CO_2 and CO gases sheds information on the state of combustion: complete or incomplete. Larger CO_2 production is attributed to the process moving toward complete combustion while more CO production indicates incomplete combustion. CO evolution at different temperatures for a 2-hours heating is depicted in Figure 5.7. For burning at 500 and 600 °C, the CO concentration was found to be below the detection limit of the gas analyser used (least count 0.01 v/v% for CO, 0.1 v/v% for CO_2). The highest concentration was measured at 700 °C. The concentration for higher temperatures viz. 800 and 900 °C was found to be lesser than that for the case of 700 °C. It may be noted that a similar trend with regard to particle generation is observed at these temperatures.

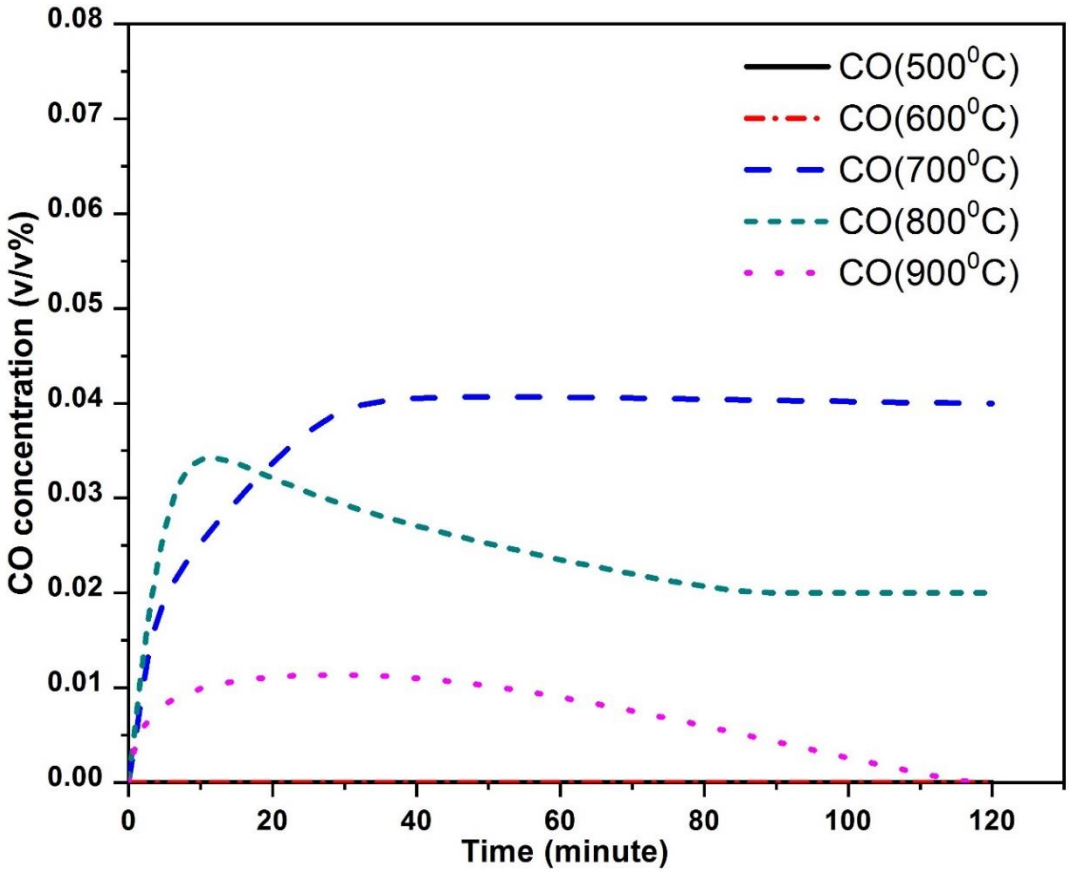

Figure 5.7: Carbon monoxide evolution at different temperatures for 2-hours graphite heating

CO_2 emission is shown in Figure 5.8. No gas was detected at 500 and 600 °C. Gas was detected at 700 °C and its concentration increased with temperature, reaching a peak value of 0.75 v/v% at 900 °C. This indicates that the reaction moves towards complete combustion at higher temperatures. The concentration values for 800 and 900 °C after the initial 30 minutes were similar, indicating that the oxidation rate reaches to its saturation limit as the burning process continues.

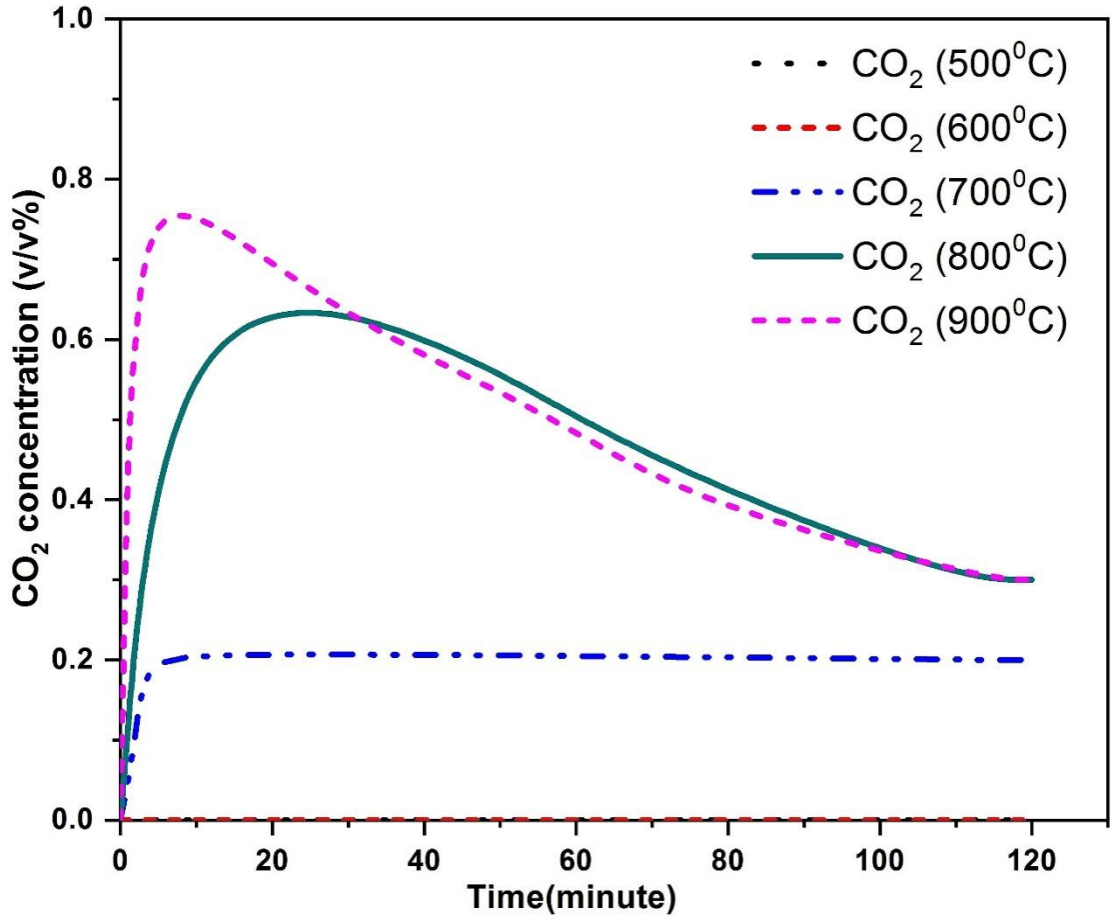

Figure 5.8: Carbon dioxide evolution at different temperatures for 2-hours graphite heating

5.1.6 Weight loss analysis

After burning for 2-hours at different temperatures, residual samples were weighed and the weight loss % was calculated. Results about the percentage of graphite burnt at

different temperature are presented in Table 5.1. These results are presented for the residual weight after 2-hours of combustion. It is seen that the weight loss is negligible at 500 °C, indicating that combustion had not started. The weight loss increased as the temperature was increased in the experiment. At 600 °C, a small weight loss was observed which marked the onset of combustion. The difference in weight loss decreased at higher temperatures (12% in the range 800 - 900 °C in comparison 42% in 700 - 800 °C). This indicates that at these higher temperatures, the combustion process was nearing saturation.

Table 5.1: Percent loss in the weight of graphite samples

Temperature (°C)	Initial weight (g)	Unburnt weight (g)	Loss (g)	% loss
500	13.43	13.33	0.09	0.68
600	13.22	12.99	0.22	1.73
700	13.29	9.64	3.84	27.44
800	13.43	4.11	9.32	69.39
900	12.51	2.33	10.17	81.30

Table 5.2 shows the weight of graphite which was converted, upon oxidation, to various products, i.e., particles, CO and CO_2. The procedure of weight calculation has been discussed in chapter 4. Maximum particle weight was obtained at 700 °C (0.15 g) along with maximum conversion to CO (0.56 g). The conversion to CO_2 was found to increase with increase in temperature. The weight loss at 600 °C indicated that combustion had already started with the formation of combustion gases. But the concentration of gases produced was too low to be sensed by the gas analyzer. Figure 5.9 shows the quantified percentage conversion into the combustion products calculated on the basis of the weight reduction during combustion. The actual weight loss was measured by weighing the residual sample after the heating process and furnace cooling up to the room temperature. This value came to be more than the calculated total weight loss (using

formulae of chapter 4) because the combustion continued even after the heating was switched off and this effect was not included in the calculations.

Table 5.2: Weight balance of combustion products

Temperature (°C)	Graphite converted to (g)			Weight loss (g)	
	Particles	CO	CO_2	Calculated	Actual
500	0.00	0.00	0.00	0.00	0.09
600	0.08	0.00	0.00	0.08	0.22
700	0.15	0.56	3.00	3.71	3.84
800	0.11	0.36	7.40	7.87	9.32
900	0.04	0.13	7.74	7.90	10.17

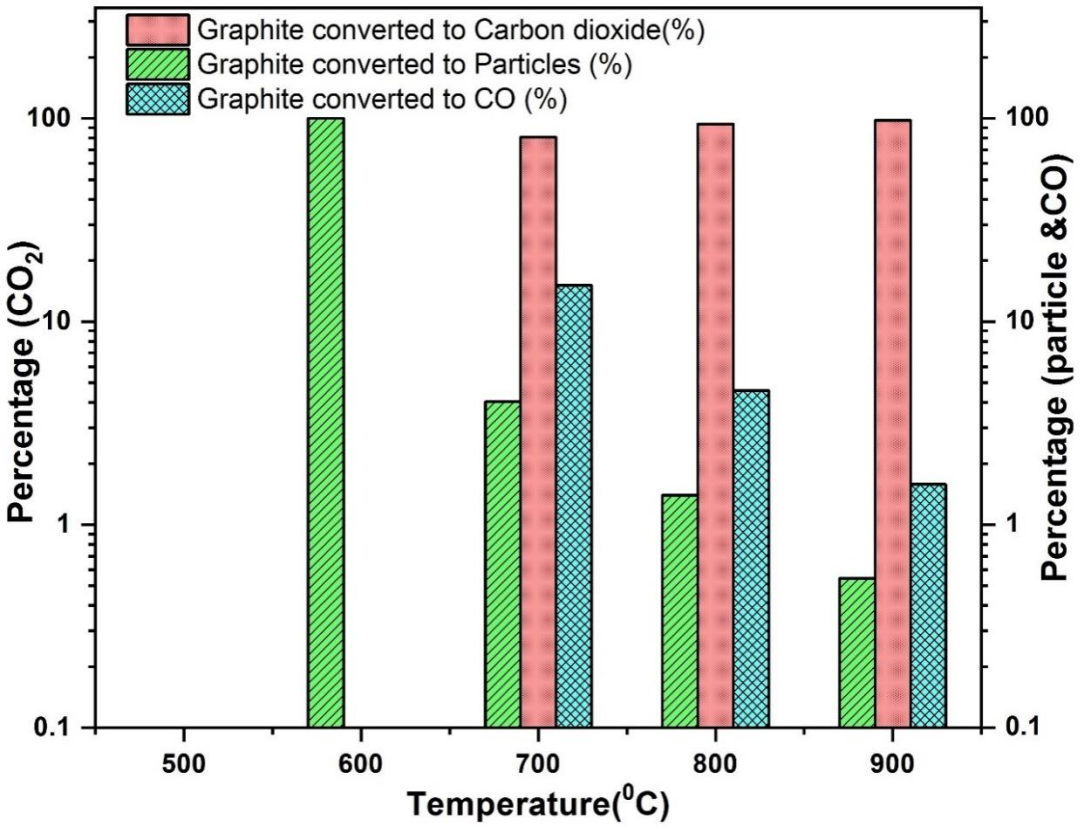

Figure 5.9: Percentage of graphite converted to combustion products

5.2 Graphite burning at different heating rates

In the present section, graphite heating was carried out at flowrates of 10, 15, 20 and 25 $Lmin^{-1}$ at four different heating rates of 2, 4, 6 and 8 °C/min. Nanoscan and Optical Particle Sizer were used to find the particle number concentration in the exhaust. A Gas Analyzer was used to measure trace gas levels (CO and CO_2). Negligible particles were observed in the OPS as compared to the Nanoscan. Hence, in the present study, only the Nanoscan results are presented.

5.2.1 Characteristics of generated particles

The total number concentration of the aerosol generated due to the burning of graphite sample at different conditions of heating rate and air flow rate is depicted in Figure 5.10. For all the cases investigated, negligible particle generation was observed below 570 °C and in every condition a peaking profile was noted. The peak of the particle concentration was lying mostly between the temperature range 600 to 800 °C. It was observed that particle generation at a specific flow rate increased by increasing the heating rate. For example, in Figure 5.10a at a flow rate of 10 $Lmin^{-1}$, the number concentration increased from 4×10^{6} to 5×10^{6} #/cm^3 as the heating rate was increased from 2 to 8 °C/min. The same trend was seen for all the flow rates considered. The peak number concentration recorded a decrease with increasing air flow rate for all heating rates. The peak number concentration decreased from about 5.13×10^{6} #/cm^3 at heating rate of 8 °C/min to around 3×10^{6} #/cm^3 at the same heating rate as the flow rate was increased from 10 to 25 $Lmin^{-1}$. The maximum concentration of particle (5.13×10^{6} #/cm^3) was observed at lowest flowrate (10 $Lmin^{-1}$) and highest heating rate (8 °C/min) in Figure 5.10a. From Figure 5.10a-d, it is also observed that the peak of maximum number concentration shifted laterally towards a higher temperature at increasing heating rate.

The details of particle generation mechanism for graphite burning are discussed in section 5.4.

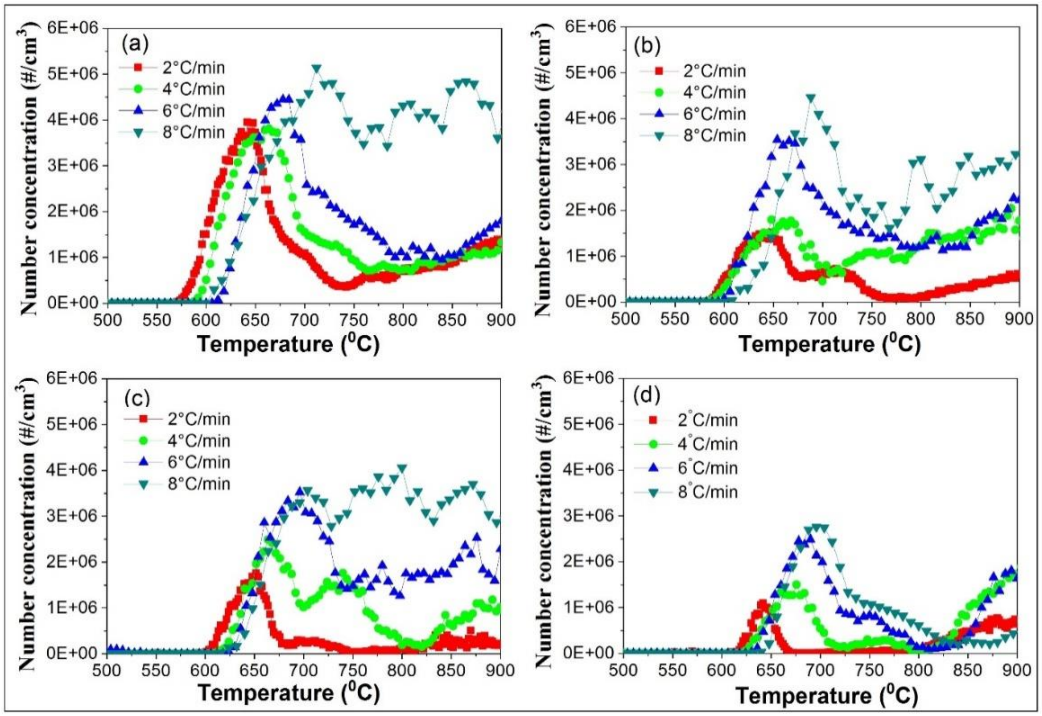

Figure 5.10: Total number concentration of generated particles at different heating rates and flow rates (a) 10 $Lmin^{-1}$ (b) 15 $Lmin^{-1}$ (c) 20 $Lmin^{-1}$ (d) 25 $Lmin^{-1}$

5.2.2 Size distribution

As stated earlier, the physical and chemical characteristics of the particles rely on their size and size distribution. Therefore, in the present section, the particle size distribution of generated graphite particles has been studied and the findings are presented in Figure 5.11a-d. For all the investigated conditions, the majority of particles were located within the nucleation range (10 - 50 nm) and accumulation range (100 - 240 nm). The particle generation/formation for the range 50 - 100 nm and 210 - 365 nm were not observed at lower heating rate values i.e. 2 and 4 °C/min at all flow rates. However, when the heating rate was increased to 6 and 8 °C/min at lower flow rates (10 and 15 $Lmin^{-1}$), the formation/generation of particles was also observed in range of 50 - 100 nm and 240

- 365.2 nm (Figure 5.11a-b). As the flow rate increases from 15 to 20 $Lmin^{-1}$ the generation of higher size bin particles of range 200 - 365 nm disappears for all heating rates (Figure 5.11c). With further increase in flow rate from 20 to 25 $Lmin^{-1}$, the particle generation/formation of both the range 50 - 100 nm and 200 - 365 nm disappears (Figure 5.11d). From the above observation, we conclude that overall generation of particle size distribution was drastically influenced by heating rate and flow rate.

At a higher heating rate, the number concentration of generated particles increased. Larger number density is reported to increase the phenomenon of coagulation resulting in generation of larger sized particles (William C. Hinds, 1999). The particles concentration and the number of particles in the larger size range decreased (shifted towards the nucleation mode (10 - 50 nm) (Figure 5.11) with an increase in the air flow rate. This observation can be explained on the basis of the fact that the combustion phenomena gets accelerated at high flow rates resulting in burning of the generated particles into smaller ones.

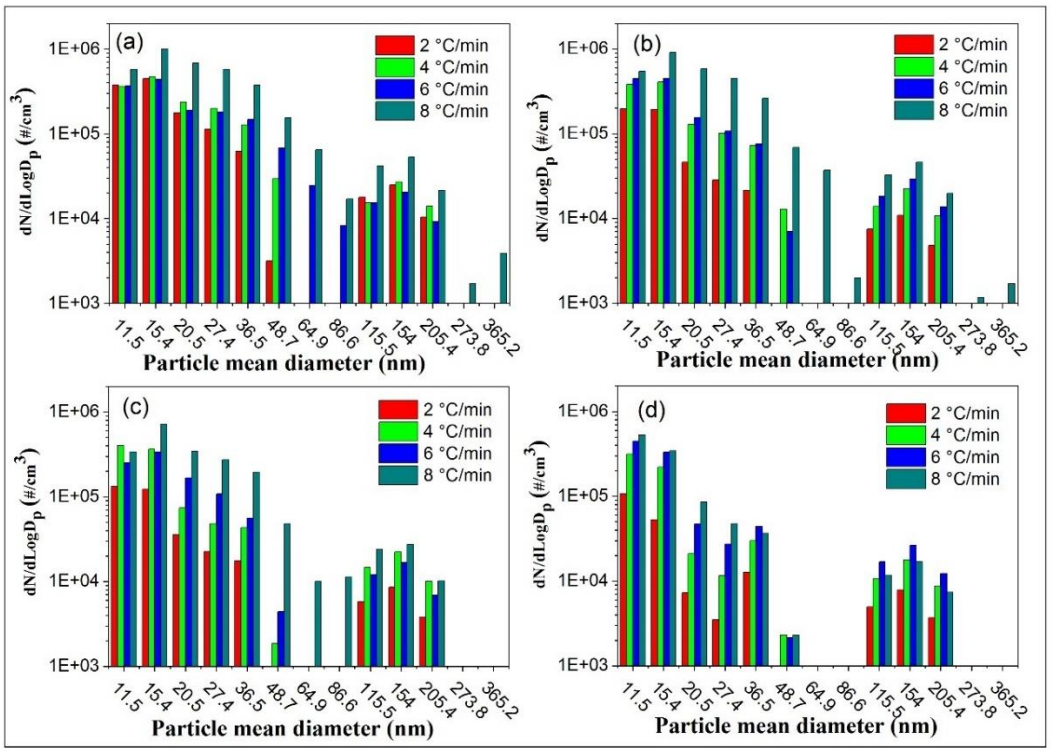

Figure 5.11: Particle size distribution at different heating rates and flow rates (a) 10 $Lmin^{-1}$ (b) 15 $Lmin^{-1}$ (c) 20 $Lmin^{-1}$ (d) 25 $Lmin^{-1}$

5.2.3 Gas analysis

In the present section, the concentration of CO gas was measured at different air flow and heating rates and the variation is depicted in Figure 5.12. For all conditions, at a temperature below 570 °C, CO emission was not detected. The peak concentration of CO increases with increasing heating rate for all air flow rates. At 10 $Lmin^{-1}$ flow rate (Figure 5.12 a), the peak concentration of CO increased from 0.11 v/v % to 0.16 v/v % when the heat rate was increased from 2 to 8 °C/min. An increase in CO gas concentration is an indication of increase in incomplete combustion. When the heating rate is high, the time available for completion of the reaction may not be sufficient, leading to larger concentration of CO. It is also observed from Figure 5.12 a-d that the concentration level of CO reduces when the flow rate was increased. This observation can be attributed to the fact that increase in flow rate provides more supply of oxygen to the sample, causing more complete burning and hence lower concentration of CO. The maximum CO gas

concentration of 0.16 v/v% was observed at a flow rate of 10 $Lmin^{-1}$ (minimum flow rate) and a maximum heating rate of 8 °C/min. This observation is consistent with the particulate concentration presented in Figure 5.10a where the maximum number concentration was reported at the lowest flow rate of 10 $Lmin^{-1}$ and highest heating rate of 8 °C/min. More incomplete combustion, manifested in larger generation of CO, also results in enhancement of number concentration of particles generated. A lateral shift of the peak CO concentration towards higher temperature with increasing heating rate for all air flow rates was also observed.

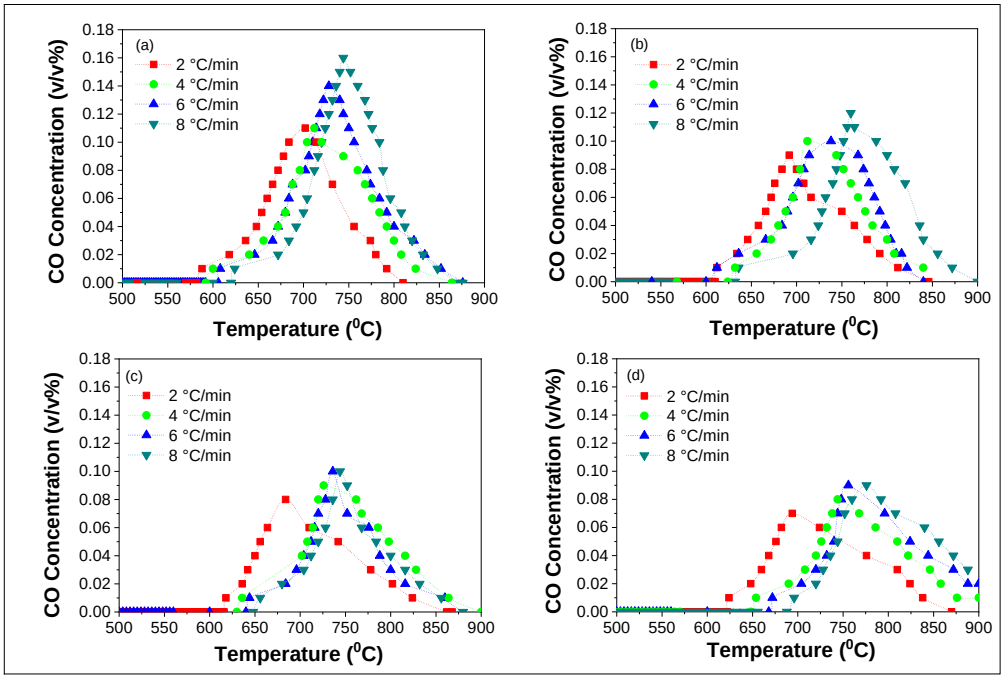

Figure 5.12: Carbon monoxide evolution at different heating rates and flow rates (a) 10 $Lmin^{-1}$ (b) 15 $Lmin^{-1}$ (c) 20 $Lmin^{-1}$ (d) 25 $Lmin^{-1}$

The CO_2 gas concentration was also measured and is presented in Figure 5.13. For all cases, CO_2 gas generation was recorded after the temperature reached about 625 °C while for CO production this temperature was about 570 °C. CO_2 concentration increased with increasing temperature and reached a steady level at around 800 °C. It indicates that the oxidation rate attained its saturation level. The higher CO_2 concentrations at lower

heating rates for all flow rates indicates availability of more time for the reaction to proceed towards complete combustion. It was also noted that peak concentration of CO_2 as well as CO shifted laterally to higher temperature with increase in heating rate. At a higher heating rate, it is expected that there would be a larger temperature difference between the temperature of the sample and the temperature recorded by the indicator due to less time available for thermal soaking of the sample. Hence at any recorded temperature and a given air flow rate, the sample would be at the highest temperature at the lowest heating rate and vice versa. As regards the effect of air flow rate, it is seen that as the flow rate is increased, an increase in generation of CO_2 is seen which occurred due to enhancement in combustion kinetics. The maximum concentration of CO_2 gas (1.5 v/v%) was measured at the highest flow (25 $Lmin^{-1}$) flow rate and at a minimum heating rate of 2 °C/min.

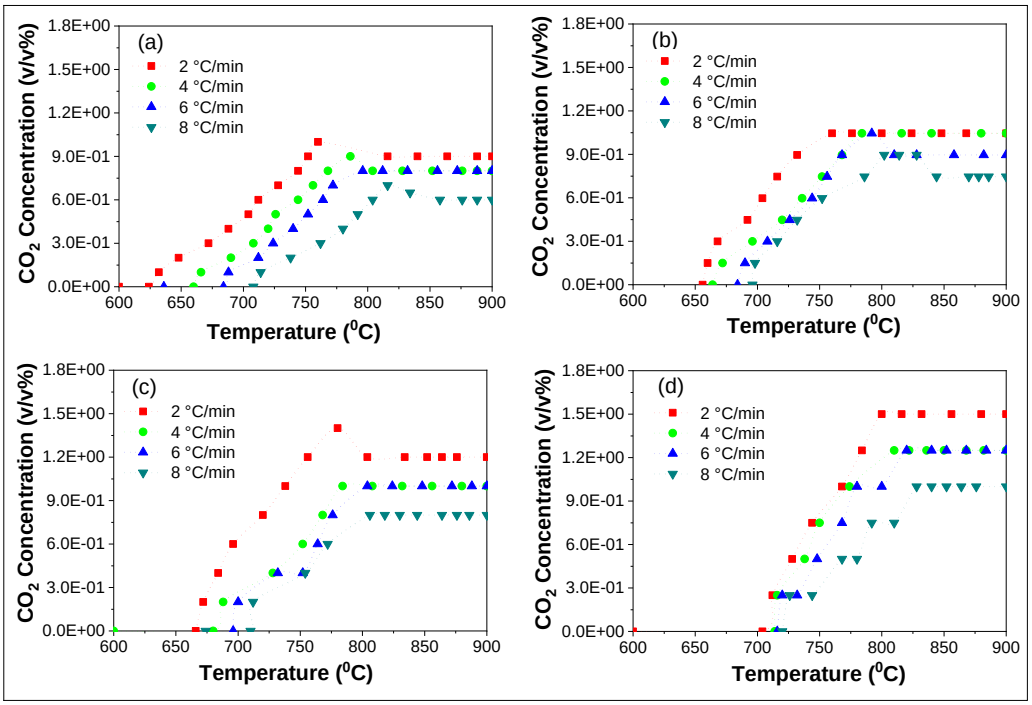

Figure 5.13: Carbon dioxide evolution at different heating rates and flow rates (a) 10 $Lmin^{-1}$ (b) 15 $Lmin^{-1}$ (c) 20 $Lmin^{-1}$ (d) 25 $Lmin^{-1}$

5.2.4 Weight loss analysis

After conducting the experiment under different conditions, the weight loss due to oxidation was measured. Figure 5.14 represents the weight loss percentage of graphite after heating at different conditions. The weight loss percentage was found to increase with rise in flow rate at a specific heating rate. It was also observed that the percentage of weight loss at a specific flowrate reduced when the heating rate was increased. This could be because the sample get less time to get uniformly heated and also higher heating rate is responsible for incomplete combustion. A highest weight loss percentage of 80% was observed at a maximum flow rate of 25 $Lmin^{-1}$ and a minimum heating rate of 2 °C/min.

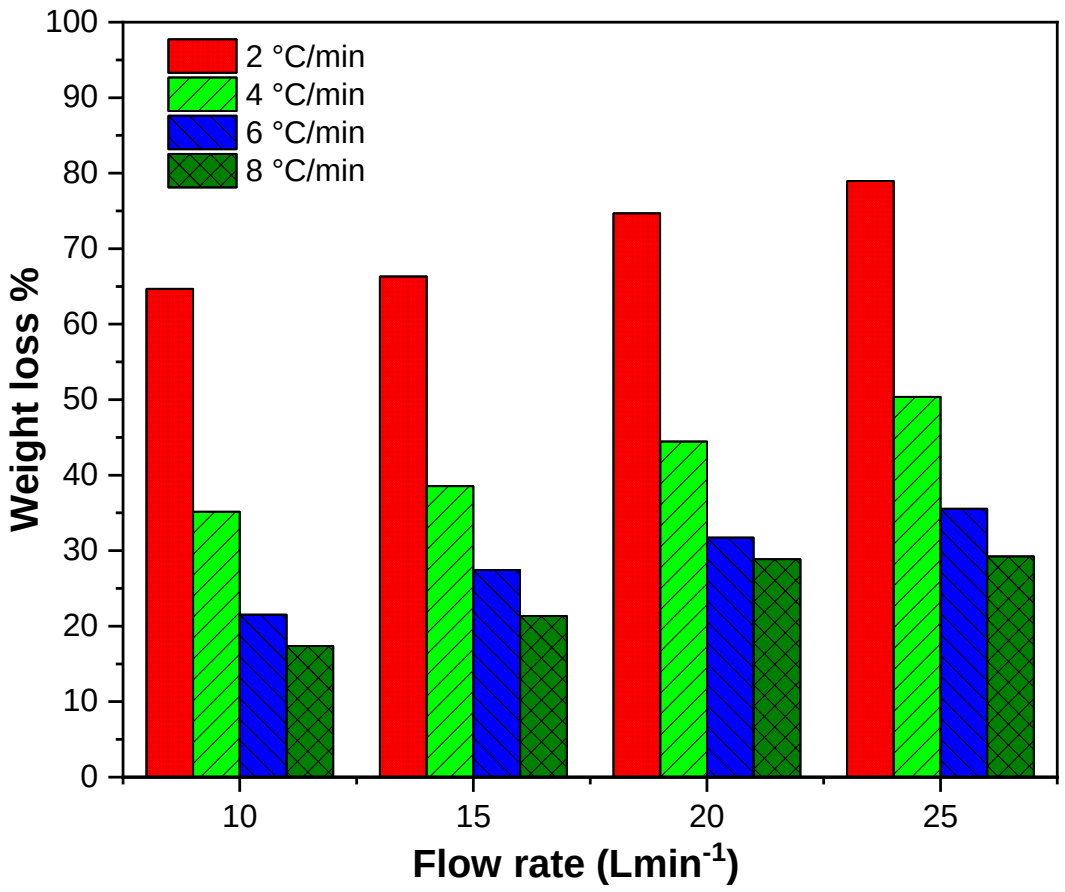

Figure 5.14: Percentage of weight loss at different heating rates and flow rates

5.3 Results for alumina coating

In case of an air ingress, use of coated graphite elements is expected to retard oxidation or particle generation. However, very little information is currently available on the characterization of aerosol produced during oxidation of alumina (Al_2O_3) coated graphite. In the present section, we focus on measuring and interpreting the role of a coating in generation of aerosol particles from graphite surface at high temperatures.

5.3.1 Effect of heating on surface morphology during oxidation

In an earlier section 5.1, we discussed the effect of burning temperature on surface morphology of graphite samples. The occurance of cavities and flakes was found to increase when the test temperature increased from 500 to 600 °C. Beyond 700 °C, the reduction in formation of flakes was attributed to a higher rate of reaction compared to oxygen diffusion. In the present work, Scanning Electron Microscopy (SEM) was used to study surface morphological transitions for residual Al_2O_3 coated graphite samples. This analysis has been presented for two cases viz. 'coated residual sample as such' and 'coated residual sample after removal of coating'. Figure 5.15a represent the SEM image of an unheated coated graphite sample. The SEM images of the residual coated graphite samples without removing the Al_2O_3 coating layer is presented in Figure 5.15b-f. It can be pointed out from these images that no significant change in the microstructure of the coating layer occurred till 700 °C (Figure 5.15a-d). Pores were seen to have formed on the coating surface at 800 °C and their number density increased at 900 °C. Also, the pore size was found to be higher at 900 °C (Figure 5.15f) as compared to 800 °C (Figure 5.15e). The modifications in the pore characteristics can be linked to the emission of CO and CO_2 gases and the generation of unburnt particles.

The coating from the residual sample was peeled off and the images of the residual samples are shown in Figure 5.16a-f. No significant change in the surface structure of graphite was seen till 700 °C (Figure 5.16a-d). At 800 °C, when pores were seen to be formed on the coating in Figure 5.15e, small cavities and flakes were formed on the surface of graphite (Figure 5.16e). With further increase in temperature to 900 °C (Figure 5.16f), cavity size increased which is indicative of an increase in graphite oxidation rate.

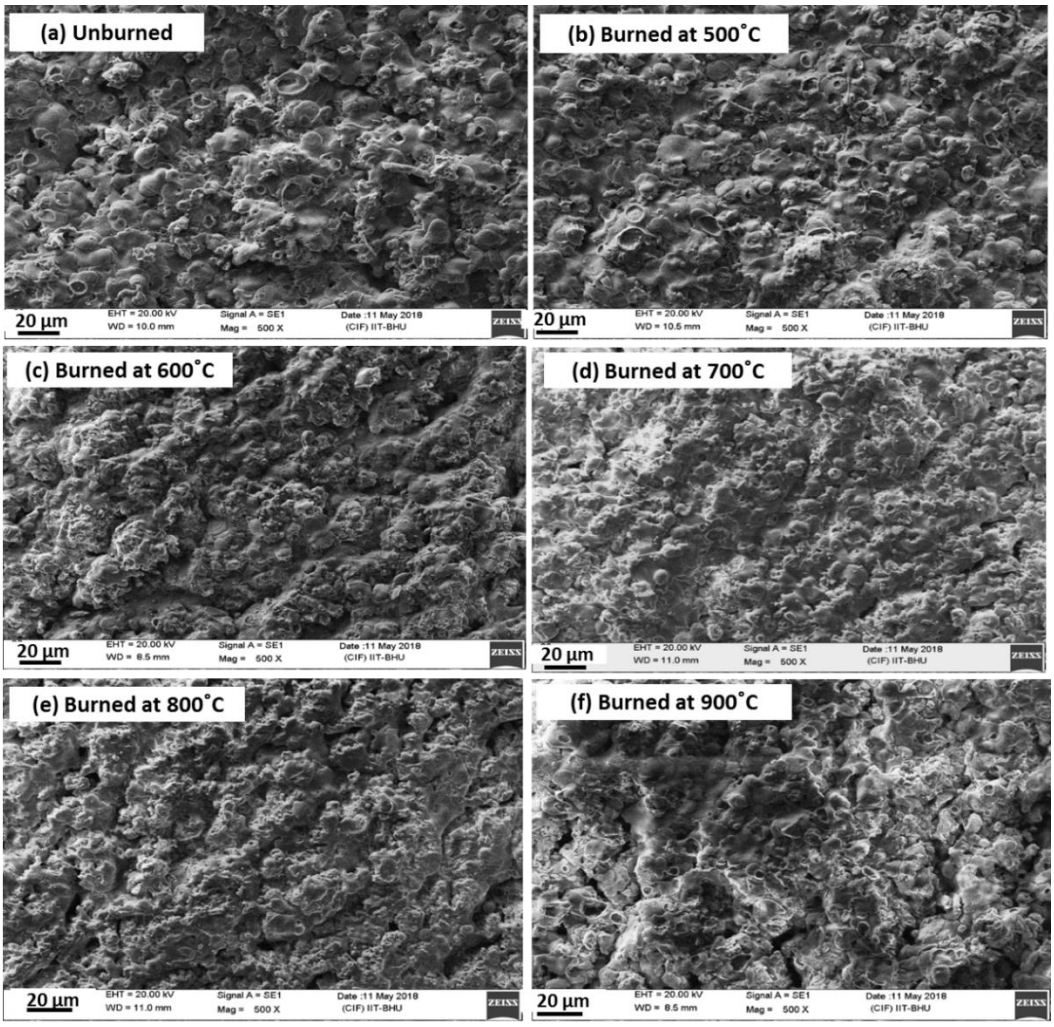

Figure 5.15: SEM analysis of residual Al_2O_3 coated graphite samples without removing coating layer

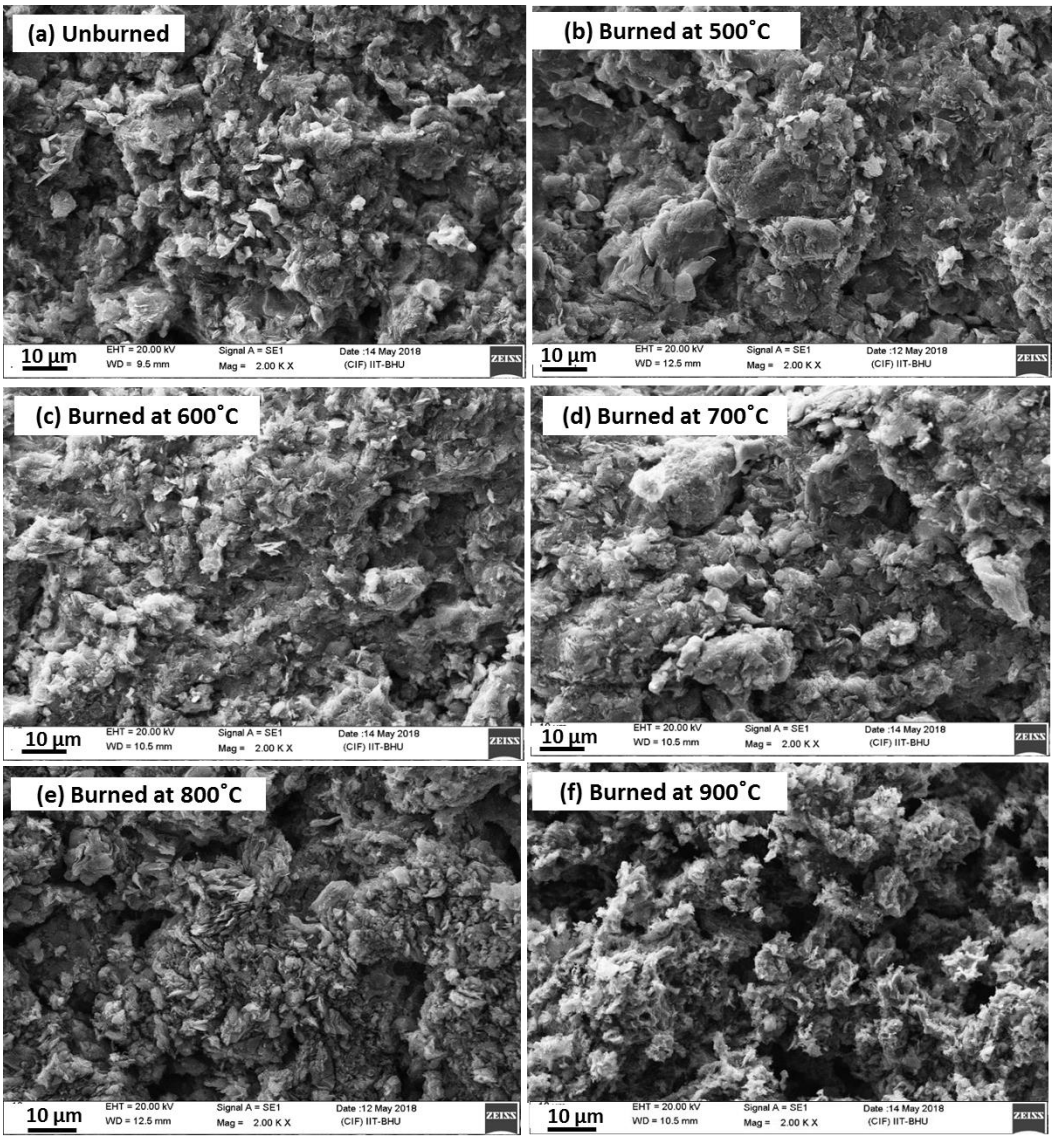

Figure 5.16: SEM analysis of residual coated graphite samples after removing coating

5.3.2 Characteristics of generated particles

A comparison of the total number concentration of aerosol particles generated due to the burning of bare graphite and Al_2O_3 coated graphite at various test temperatures is plotted against time and shown in Figure 5.17. For all investigated temperatures, a peaking behavior is observed for the number concentration profile. In the beginning of the combustion for bare graphite as well as Al_2O_3 coated samples, the particle generation was relatively higher. However, with continued heating at constant temperature, the

particle emission started declining for all the cases. In the case of heating of bare graphite at 500 °C, negligible particle generation (similar to background number concentration) was observed. At 600 °C, number concentration was seen to be rising rapidly at initial times, decreasing slowly but steadily afterwards. The peak number concentration measured for this case was 1.4×10^6 #/cm^3. Similar kind of behavior was followed by the number concentration profile at 700 °C. For this case, peak number concentration was found to be highest 5.3×10^6 #/cm^3 among the tested temperatures. After 700 °C, peak number concentration was found to be lesser relatively. Overall, the peak number concentration was found in the range of 0.8×10^6 - 7.8×10^6 #/cm^3 for entire experiments. When Al_2O_3 coated graphite was heated for the same conditions, particle generation was not evident till 700 °C, reflected in the measured number concentration being in the same range as the background number concentration. This implies that the coating acts successfully as a barrier to the diffusing oxygen, preventing the structural integrity of the graphite sample. However, considerable particle generation was observed during initial stages of heating at 800 °C indicating the onset of pore generation in the coating. With further increase in temperature to 900 °C, sporadic increase of number concentration at initial times continued. This is again an indication of increasing diffusional influx of oxygen at high temperatures, probably due to the increase in porosity and pore size of the exposed sample. It can also be seen in Figure 5.17d-e that the generation of particles from the coated surface occurred only for approximately 20 minutes of continuous heating after which the number concentration decreased back to the background levels. During oxidation induced burning, not only particles but combustion gases also get generated. These are expected to get trapped in the pores of the coating. Such an occurrence is expected to inhibit particle emission from the underlying graphite by retarding the diffusion of oxygen to graphite.

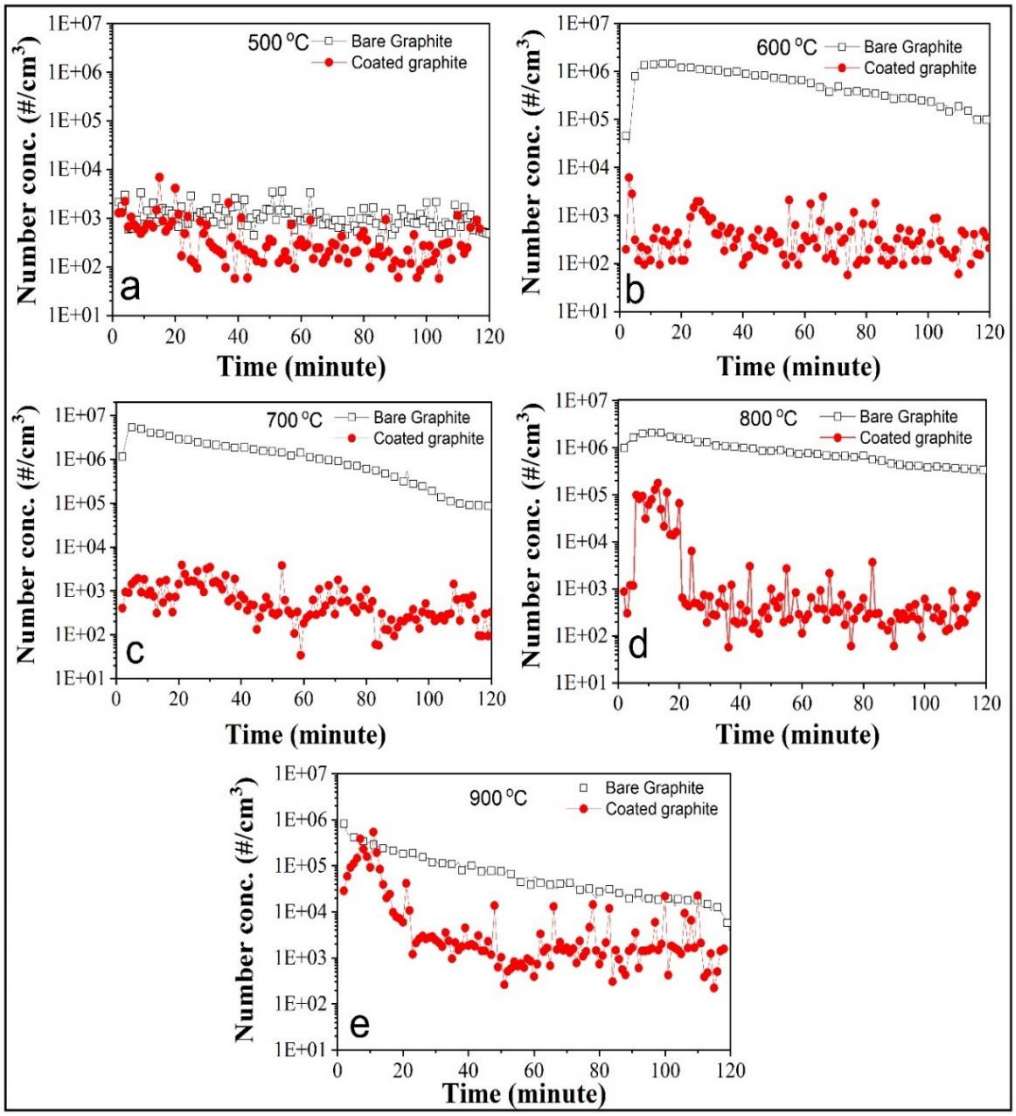

Figure 5.17: Particle generation in bare and coated graphite at different temperatures

5.3.3 Size distribution

The present section focusses on the study of the number size distribution of the generated particles from bare and coated samples. Figure 5.18a, represents the background particle number size distribution (averaged over 2-hours) along with error bar (±10%), when no sample was inserted in the heating tube. The averaging for other cases was done for the times when the number concentration was higher than the background number concentration value. For example, in Figure 15.7d, the generation of

particles from the coated surface occurred only for approximately 20 minutes, after which the concentration decreased back to the background levels, Hence, an average was calculated for a time period of 20 minutes and is shown in Figure. 15.8e. For the heating temperature of 500 °C (Figure 5.18b), the number size distribution of the generated particles from bare and coated graphite remained more or less similar. For 600 °C and 700 °C, a difference in terms of particle number size distribution for bare and coated graphite can be noted (Figure 5.18c-d). Whereas the number concentration for all the bin sizes was found to be higher than background distribution for the case of bare graphite, readings were within the error bar of background particles, for the coated graphite case. This means that there was no particle generation within this temperature range and the coating was successful in cutting off the oxygen supply to the underling graphite surface at temperatures ≤ 700 °C.

However, when temperature was raised above 700 °C, increased number concentration was observed for the case of coated graphite (Figure 5.18e and 5.18f) as well, confirming that graphite oxidation occurs above 700 °C. However as seen in Figure 5.17, particle generation continued for the entire burning period for bare graphite and was limited to smaller time scales for coated graphite samples. In addition, some differences in features of number size distribution can also be noted. Whereas the particle number concentration was insignificant in 50 - 100 nm size range (except at 700 °C) for bare graphite, particles in all sizes were observed for coated graphite. Number concentration in all size ranges for coated graphite at 800 and 900 °C was found to be similar but lesser than that for bare graphite burning at 700 °C. The pathways of particle generation and the respective mechanisms have been explained in a later section (section 5.4).

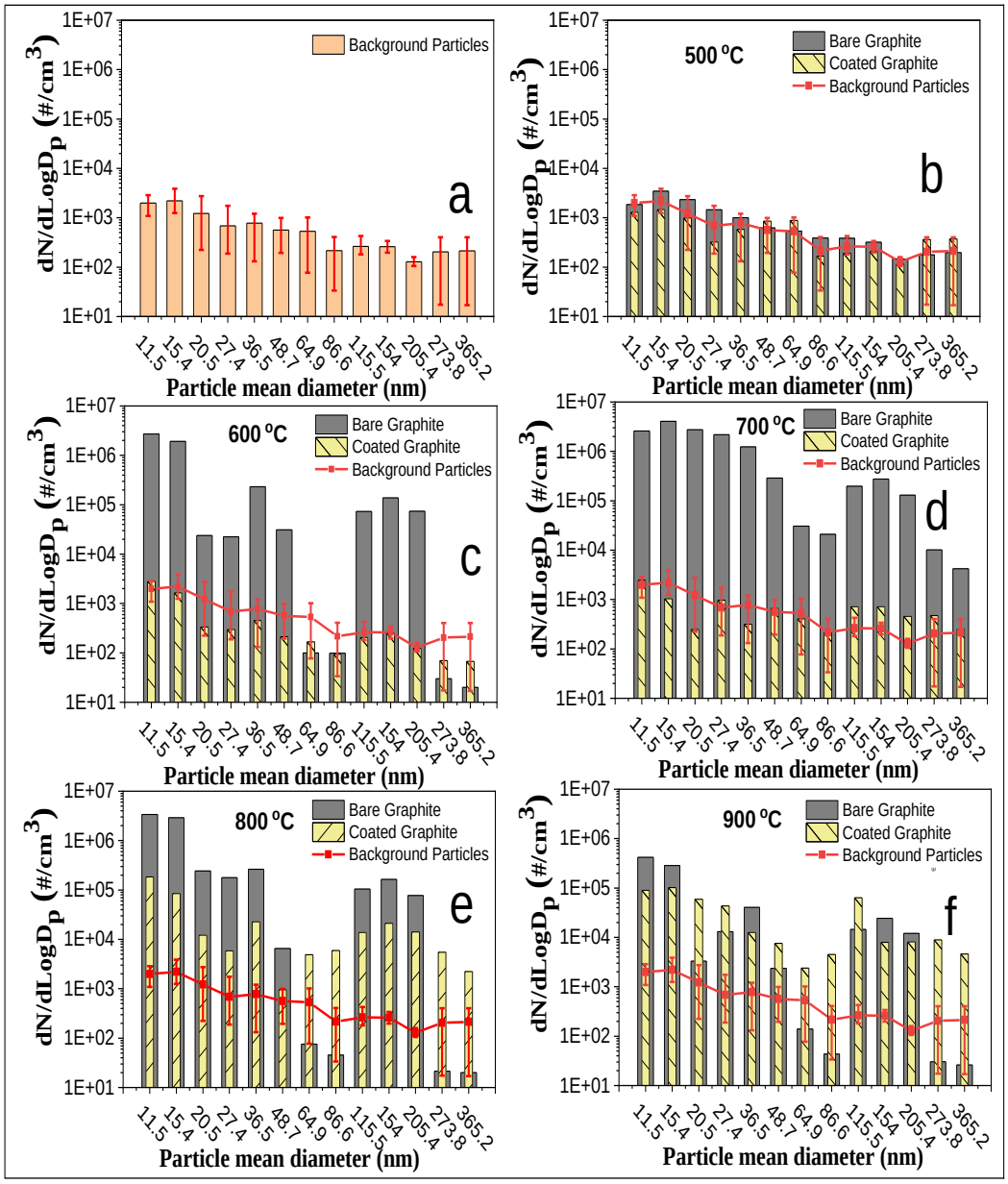

Figure 5.18: Particle size distribution for generated particles from bare and coated graphite samples

5.3.4 Gas analysis

The temporal evolution of CO and CO_2 gas concentration is shown in Figure 5.19 and Figure 5.20. CO gas was not measured by the instrument for the burning temperatures of 500 and 600 °C for bare as well as coated samples. For the case of bare graphite heating at 700 °C, emission of CO gas was observed which was found to saturate after ≅ 30 minutes. CO concentration for this case was highest compared to the burning

temperatures of 800 and 900 °C. Evolution of CO gas concentration indicated that the maximum incomplete combustion occurred at 700 °C. This observation is also in agreement with the maximum particle number concentration measured at this temperature (See Figure 5.17). However, the transition temperature was found to be higher for the case of coated graphite samples. For coated graphite, CO concentration was not measured by the analyzer till 700 °C. This is due to the reduction of graphite oxidation resulting from the barrier to influx of oxygen through the coating thickness. For higher temperatures (900 °C), CO concentration was found to be higher as compared to that for 800 °C. It is proposed that at these temperatures, formation of pores leads to the transport of oxygen to the graphite surface resulting in combustion and the formation of CO. The transition temperature on the basis of CO gas signature was found to be higher for coated graphite sample. Also, the CO gas concentration at the maximum tested temperature i.e. 900 °C for the coated graphite case was observed to be lesser than the maximum CO gas concentration (at 700 °C) measured for bare graphite. This shows that incomplete combustion was lesser for the case of coated samples even when the burning occurred at 200 °C higher temperature than the bare graphite sample.

The temporal evolution of CO_2 gas concentration for all the cases (bare and coated samples at different burning temperatures) is shown in Figure 5.20. For the bare sample, no CO_2 emission was measured at 500 and 600 °C. Afterwards, CO_2 gas concentration was found to be increasing with the burning temperature. However, small difference of CO_2 gas concentration at later times for 800 and 900 °C indicates non-dependency of CO_2 emission on temperature above a threshold temperature. For coated graphite samples, CO_2 production started only at 900 °C. It can also be seen that CO_2 gas concentration for this case was lesser than the minimum recorded concentration for bare graphite. The results based on the temporal profile of CO_2 emission reinforce the argument that the

alumina coating protects the graphite surface against structural degradation at high temperatures. However, at 900 °C or higher temperatures (not studied in this work), pore formation would lead to the increase in oxygen influx to the graphite surface resulting in structural damage even for coated samples.

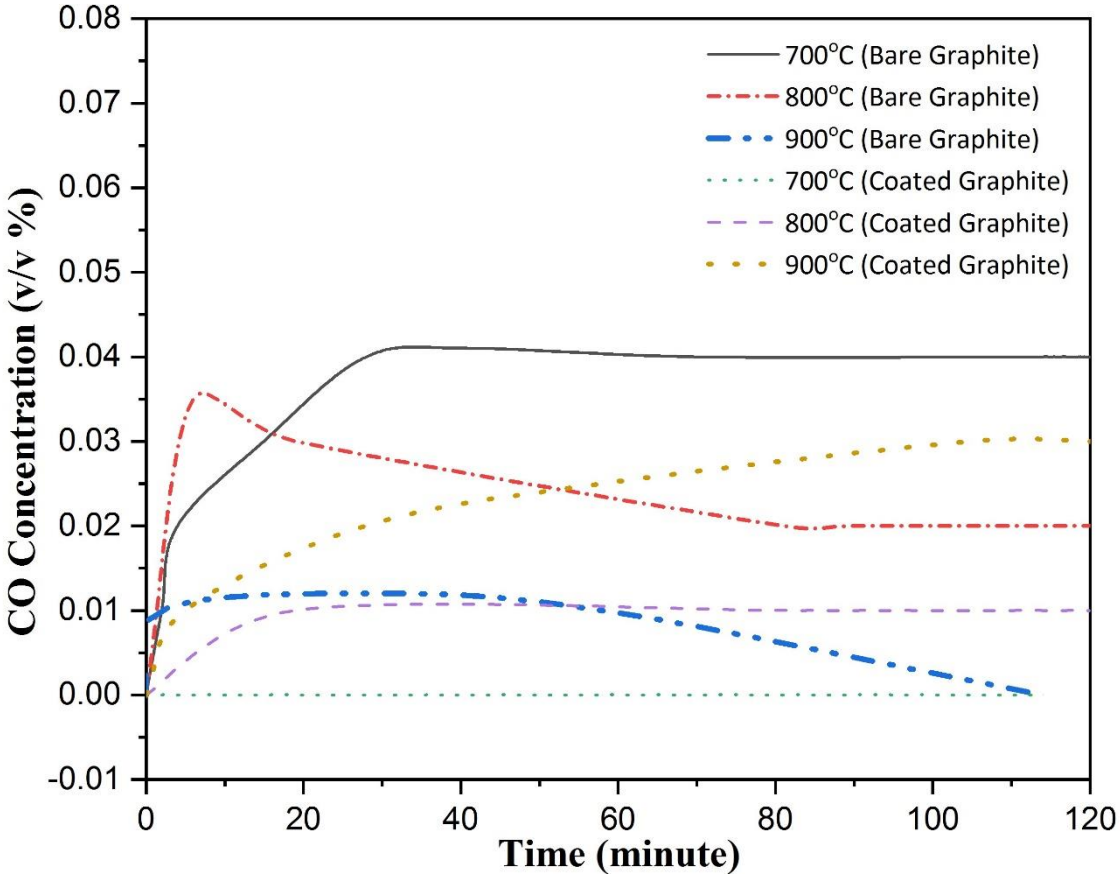

Figure 5.19: Carbon monoxide generation at different temperatures for bare and Al_2O_3 coated graphite

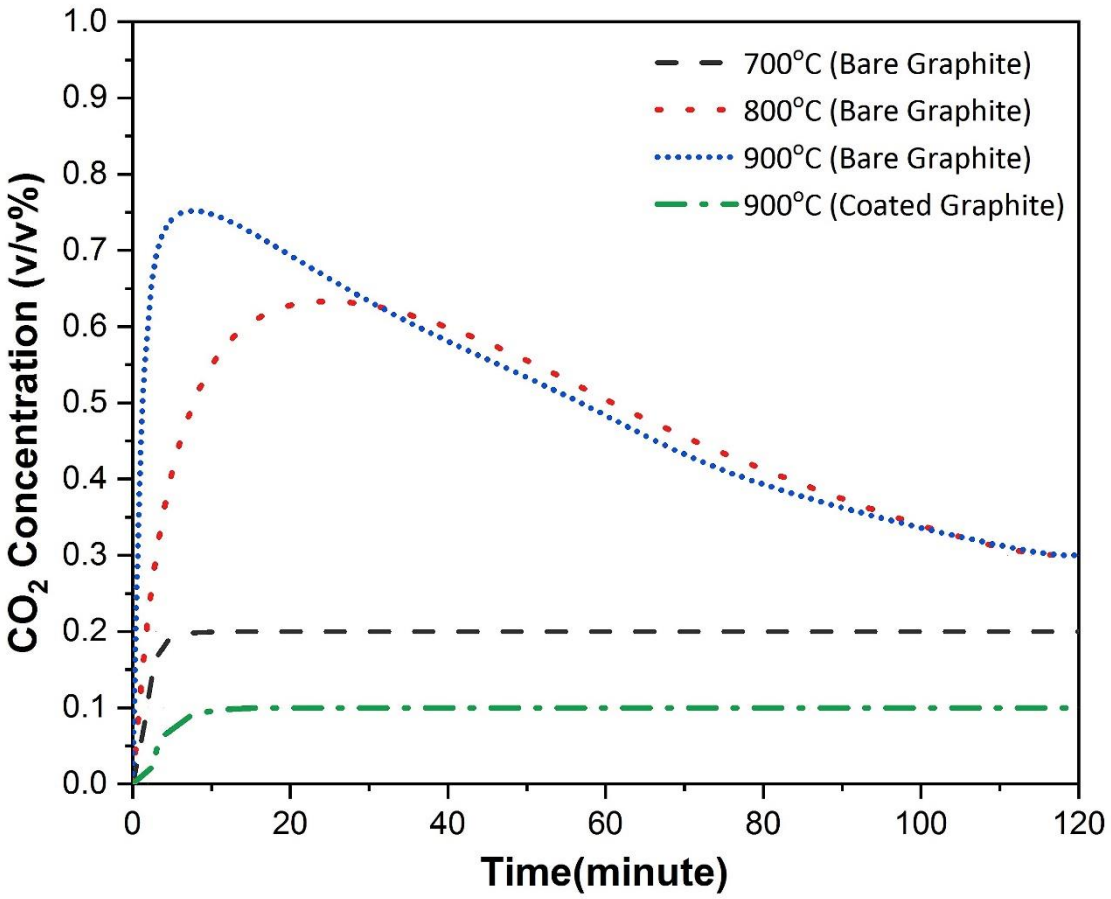

Figure 5.20: Carbon dioxide generation at different temperatures for bare and Al_2O_3 coated graphite

5.3.5 Weight loss analysis

After burning for 2-hours at different temperatures, residual samples (bare as well as coated) were weighed and the weight loss was calculated for all cases. The weight loss (%) for all cases of experimental test matrix has been plotted in Figure 5.21. For bare graphite, the weight loss increased with the burning temperature leading to almost a reduction of approx. 80% weight of the sample for 900 °C. However, the rate of increase of weight loss was found to be higher when compared for transition from 700 to 800 °C (i.e. actual weight loss difference at 700 and 800 °C is 5.48 g) and from 800 to 900 °C (weight loss difference at 800 and 900 °C is 0.85 g). For coated graphite samples, weight

loss was negligible even at 800 °C due to the reason stated above. Weight loss was noted to be approximately 10% at 900 °C for this case.

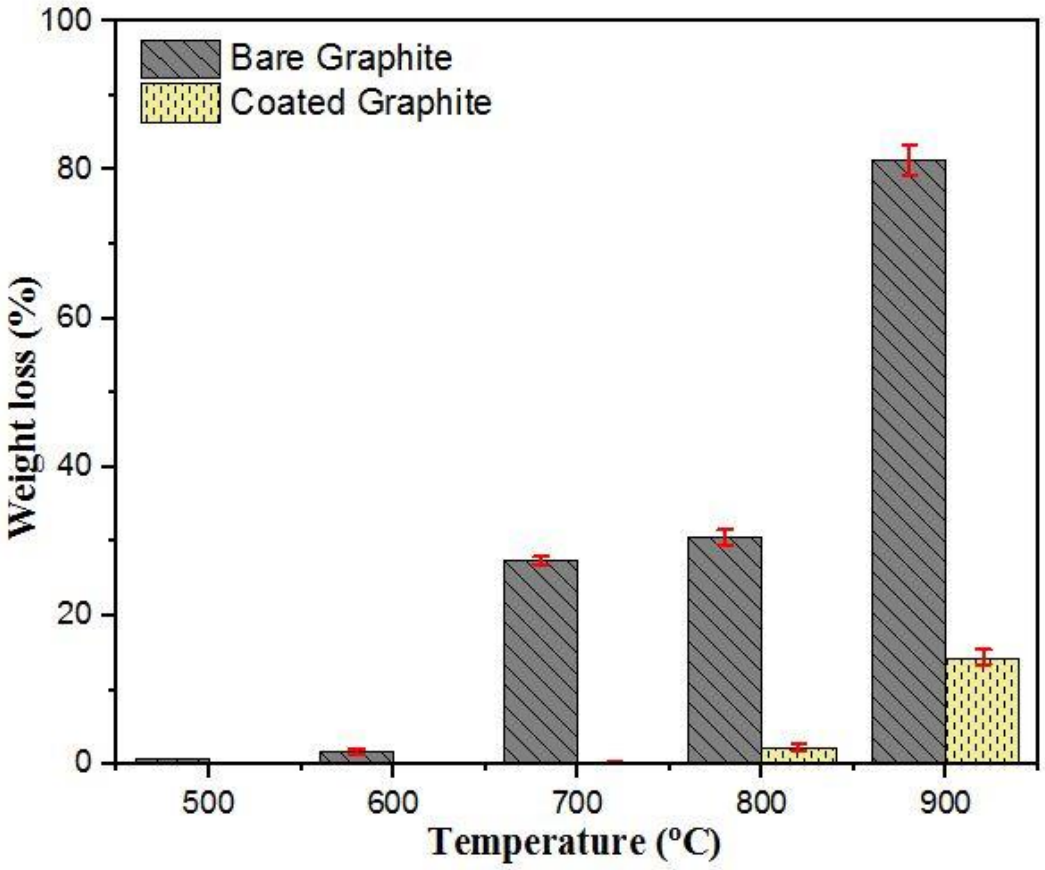

Figure 5.21: Weight loss percentage in bare and coated graphite samples after burning for 2-hours

5.3.6 XRD analysis of residual sample

XRD analysis was also performed for residual samples for investigating the change in crystal pattern, if any. Figure 5.22a and 5.22b represent the XRD analysis of bare graphite and coated graphite samples after burning at different temperatures, respectively. No structural changes and internal stress generation was found for both these cases. The XRD pattern was seen to be matching with the standard graphite diffraction pattern (JCPDS card number: 08-0415). It was expected as the recrystallization temperature of graphite is approximately 1300 °C. (Blackman and Ubbelhode, 1962), not achieved in the present work.

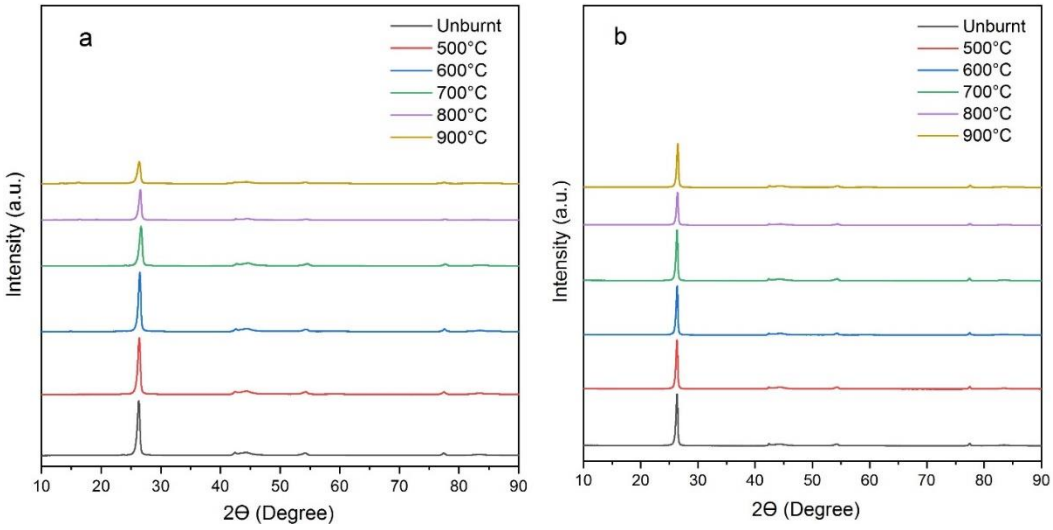

Figure 5.22: XRD of (a) bare and (b) coated graphite after burning at different temperatures

5.4 Discussion

5.4.1 Mechanism of particle generation

Particles generated during combustion process can be segregated into two categories. The first category refers to ash containing non-combustible constituents (other than carbon and hydrogen) of the sample. The second category consists of carbonaceous particles and is formed by incomplete combustion of the sample (Flagen and Seinfeld, 1988). Block diagram of particle generation categories is shown in Figure 5.23. As the present study used pure a graphite sample, particles were formed by incomplete combustion of the sample only. During graphite oxidation, various oxides of carbon (C_xO_y: CO, C_3O_2, C_4O_2 etc.) are formed (Flagen and Seinfeld, 1988; Haynes and Wagner, 1981). In addition, a large amount of heat gets liberated on the surface of graphite as an effect of CO and CO_2 formation (exothermic reaction). Under purging flow conditions, these hot vapors get quenched thermodynamically and nucleate. The nucleated particles further grow as an effect of coagulation and condensation phenomenon (Figure 5.24). As seen from results discussed in previous sections, graphite particles were generated mostly

in the nucleation mode (10 - 50 nm) and accumulation mode (> 100 nm) size ranges. The smaller mode particles were generated via evaporation-condensation and evolved with time due to coagulation and condensation process (Deuerling et al., 2010; Goudeli et al., 2016; William C. Hinds, 1999). However, the larger size range particles could be the unburnt carbon particles residing on (or inside) the sample which got carried away by gases and the carrier flow. Coagulation can also be attributed to the particles observed in higher size ranges (Figure 5.25).

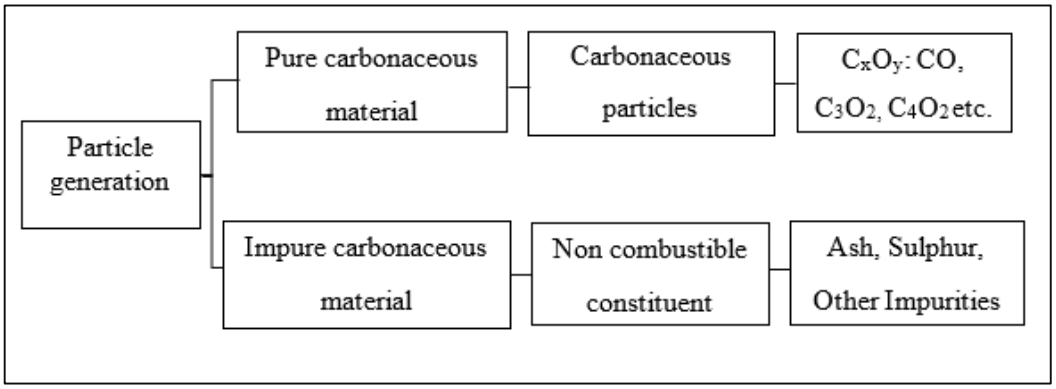

Figure 5.23: Block diagram of categories of particle generation

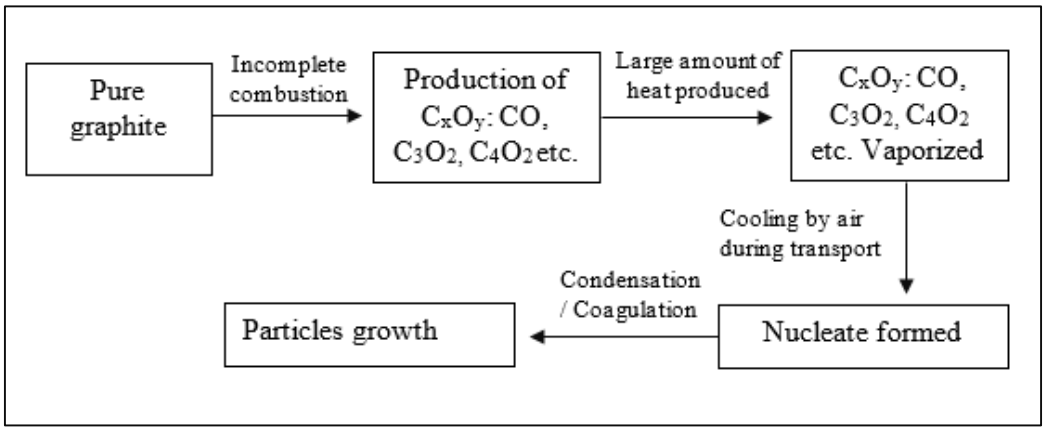

Figure 5.24: Block diagram of graphite particle formation

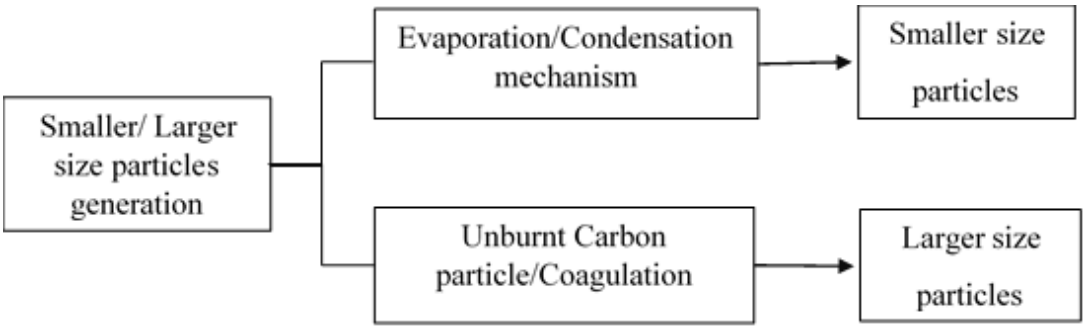

Figure 5.25: Block diagram of smaller/larger particle formation

5.4.2 Oxidation mechanism in graphite

As discussed earlier (chapter 1) that reactions occur in graphite in three regimes: the chemical regime, the controlled boundary layer regime and the controlled in-pore diffusion regime. In addition, two models for solid- fluid reaction: progressive model and shrinking core model have also been discussed earlier. In the present study it is assumed that below 600 °C temperature, reaction in graphite lies in the chemical regime. In this lower temperature domain, progressive model for solid- fluid reaction plays a significant role. In this model, the reactant gas enters and reacts throughout the sample at all time with different rates for different locations. The reactant is converted continuously and progressively throughout the sample (Morin et al., 2017). At higher temperatures i.e. above 800 °C, reaction in graphite lies in boundary layer regime. In this domain, the shrinking core model play a vital role and the reactions first start at the outer surface of the particle. The reaction zone then moves inside the reacting core surface, leaving behind combustion products. The core of the particle shrinks in size with time during the reaction (Ahn and Choi, 2017; da Rocha et al., 2013). However, for temperature range between 600 - 800 °C, reactions occurring in graphite lie in the pore diffusion regime. The transition from progressive model to shrinking core model takes place at a temperature that is called transition temperature. The block diagram of reactions in graphite is shown in Figure 5.26.

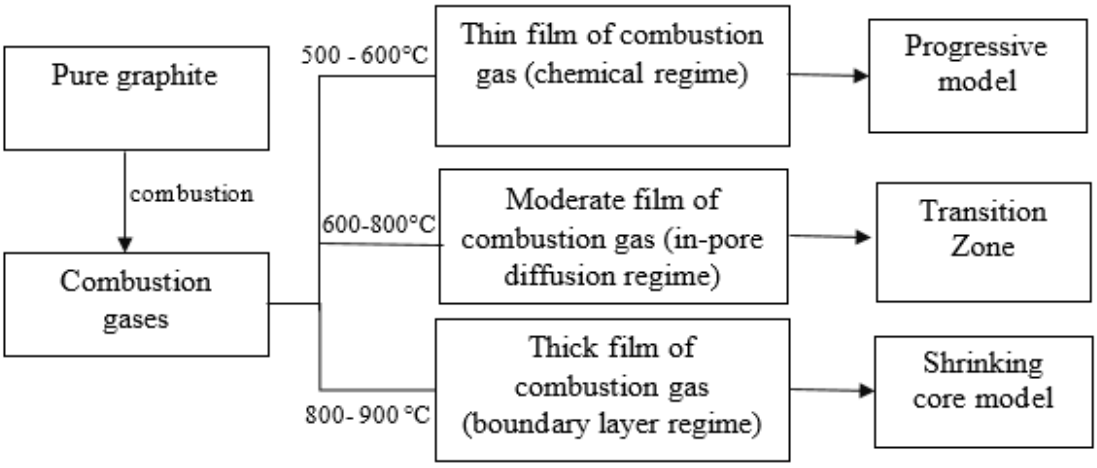

Figure 5.26: Block diagram of reaction occurs in graphite

5.4.3 Effect of heating at constant temperature on the generation of particles

The results obtained in the present work have been explained based on the well-established progressive, transition zone and shrinking core models of combustion. At 500 °C, the combustion of sample had not started, resulting in negligible particle generation. Burning of sample started at 600 °C but the chemical kinetics was slow. It is proposed that a thin layer of combustion gases (CO and CO_2) would form, surrounding the sample, though in a very small quantity and not recorded by the gas analyser. In such a situation, oxygen would penetrate deeper into the sample resulting in formation of flakes throughout the sample and surface weakening. Particle generation also started at this temperature but not in all size ranges. When the temperature was increased to 700 °C (transition zone), CO and CO_2 were observed as signatures of incomplete and complete combustion, respectively. Evaporation-condensation phenomenon resulted in particle generation (via incomplete combustion generated carbon sub-oxides) in nucleation mode size range. However, the larger size range particles could be the unburnt carbon particles, which got carried away by gases and the carrier flow. Some larger particles are formed by coagulation of particles. Highest particle generation rate was recorded for 700 °C,

which can be correlated with the generation of incomplete combustion products. Chemical reactivity increased at 800 °C resulting in a thick layer of gas film surrounding the sample. This in effect offered more resistance to oxygen diffusion (compared to lower temperature cases). Increase in CO_2 concentration and decrease in CO concentration indicated the dominance of complete combustion. Lesser amount of incomplete combustion products and larger thickness of film over the surface affected the particle generation rate which was observed to be lower than 700 °C. This phenomenon (lesser particle generation rate) continued at 900 °C where combustion rate was highest among the tested temperatures. Block diagram of particles generation at different temperature is shown in Figure 5.27.

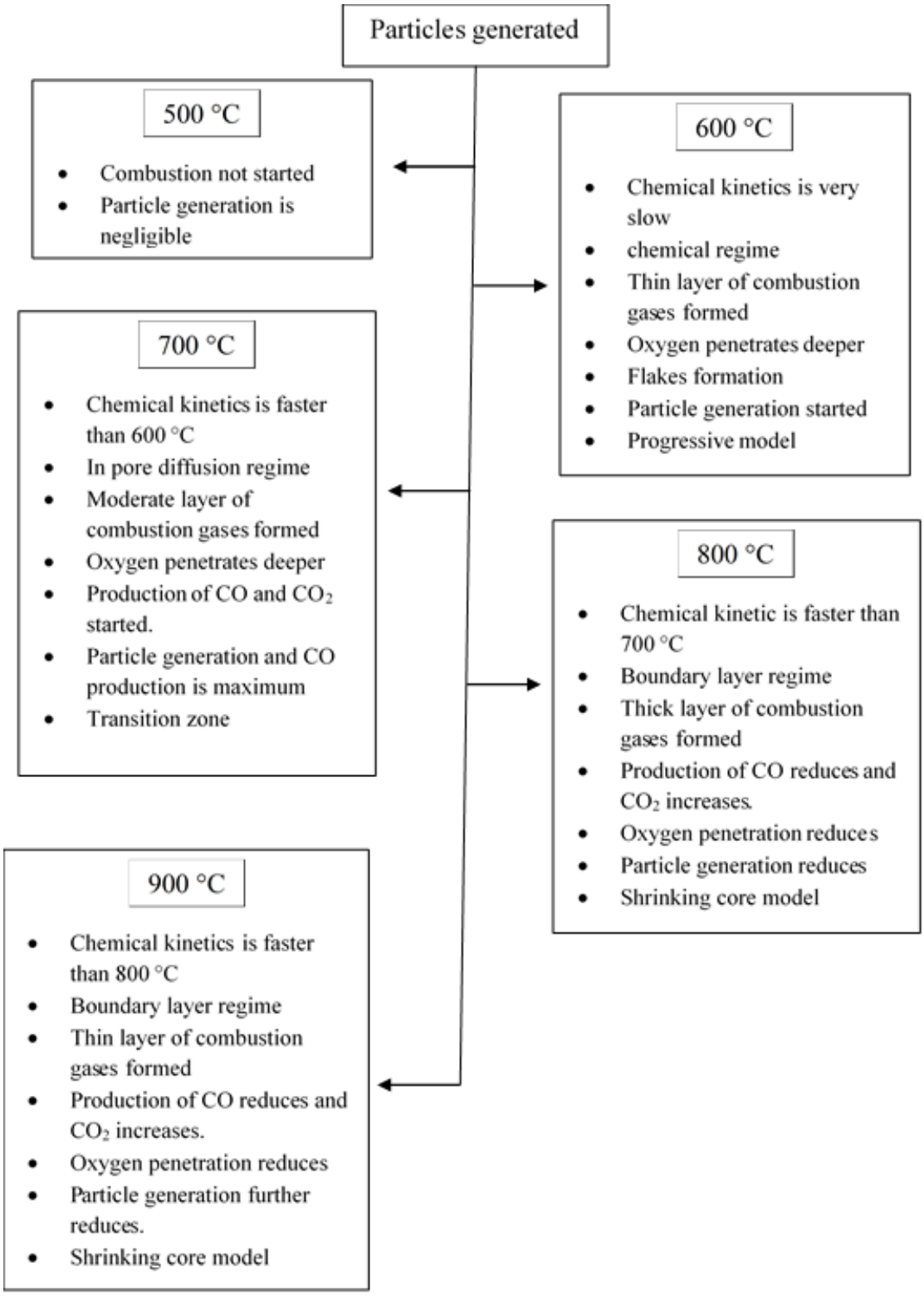

Figure 5.27: Block diagram of particle generation at different temperatures

5.4.4 Effect of heating rate on the particle generation

When graphite samples were burnt at different heating rates, the peak of the particle concentration and CO was mostly lying between the temperature range 600 to 800 °C (Figure 5.10). As discussed above, in this temperature range, oxidation of graphite was controlled by in-pore diffusion regime (transition zone). In this range, the chemical kinetics as well as the diffusion of oxygen into the sample is sufficiently high. This results in incomplete combustion leading to higher CO and particle generation. However, above 800 °C, oxidation is controlled by boundary layer regime. Reactions occur at the surface of graphite leading to decrease in CO and particles concentration.

The graphite activation energy also plays a significant role in particle generation. The graphite-oxidation activation energy in air rises to nearly 700 °C, then begins to decrease (Kane et al., 2013). As already discussed, the activation energy is a direct measurement of the thermodynamic energy barrier to the reaction. It means that around 700 °C, there is highest energy barrier for graphite oxidation and maximum incomplete combustion takes place. So the peak of particulate matter number concentration and CO generated in all test conditions was produced in the range of 600 to 800 °C. Above 800 °C, oxidation of graphite increases and the reaction proceeds towards complete combustion (low activation energy). A reduction in the sample dimensions and formation of deactivation sites at higher temperatures could also be responsible for lesser particles generation as the combustion process progresses (Radovic et al., 2011).

Summary

In the present chapter, the behaviour of aerosol generation and its characterization at different heating conditions during burning of (a) Bare Graphite at constant temperature (b) Bare Graphite at variable heating rate and (c) Alumina Coated Graphite heating at different conditions (i.e. variable heating rates and flow rates) was studied.

The following are some salient observations:

- In the case of bare graphite burning at constant temperature, the maximum concentration of CO and particles was produced at 700 °C.
- The flaky characteristics of graphite surface disappear and fused-type surface characteristic come into existence at 700 °C, indicating a transition temperature.
- The highest concentration of CO and particle was found in the range of 600 - 800 °C when the bare graphite was heated at different heating rates.
- Maximum number of particles were generated at highest heating rate (8 °C/min) and lowest flow rate (10 $Lmin^{-1}$) for gradually heating graphite.
- Alumina coating protect graphite against oxidation up to 700 °C and also reduces the overall particle generation.
- Maximum concentration of particles and CO gas was obtained for alumina coated graphite at 900 °C.

References

Ahn, H., Choi, S., 2017. A comparison of the shrinking core model and the grain model for the iron ore pellet indurator simulation. Comput. Chem. Eng. 97, 13–26. https://doi.org/10.1016/j.compchemeng.2016.11.005

Blackman, L.C.F., Ubbelhode, A.R., 1962. Stress recrystallization of graphite. Proc. R. Soc. London. Ser. A. Math. Phys. Sci. 266, 20–32. https://doi.org/10.1098/rspa.1962.0044

da Rocha, D., Paetzoldb, E., Kanswohl, N., 2013. Process intensification the shrinking core model applied on anaerobic digestion. Chem. Eng. Process. Intensif. 70, 294–300. https://doi.org/10.1016/j.cep.2013.05.003

Deuerling, C.F., Maguhn, J., Nordsieck, H.O., Warnecke, R., Zimmermann, R., 2010. Measurement system for characterization of gas and particle phase of high temperature combustion aerosols. Aerosol Sci. Technol. 44, 1–9. https://doi.org/10.1080/02786820903325402

Flagen, R.C., Seinfeld, J.H., 1988. Fundamental of air pollution engineering, Prentice - Hall, Inc. Englewood Cliffs, New Jersey. https://doi.org/10.1016/j.ijcard.2015.09.043

Goudeli, E., Eggersdorfer, M.L., Pratsinis, S.E., 2016. Coagulation of agglomerates consisting of polydisperse primary particles. Langmuir 32, 9276–9285. https://doi.org/10.1021/acs.langmuir.6b02455

Haynes, B.S., Wagner, H.G., 1981. Soot formation. Prog. Energy Combustion Sci. 7, 229–273.

Kane, J.J., Contescu, C.I., Smith, R.E., Strydom, G., Windes, W.E., 2017. Understanding the reaction of nuclear graphite with molecular oxygen: Kinetics, transport, and structural evolution. J. Nucl. Mater. 493, 343–367. https://doi.org/10.1016/j.jnucmat.2017.06.001

Kane, J.J., Karthik, C., Ubic, R., Windes, W.E., Butt, D.P., 2013. An oxygen transfer model for high purity graphite oxidation. Carbon N. Y. 59, 49–64. https://doi.org/10.1016/j.carbon.2013.02.053

Morin, M., Pécate, S., Masi, E., Hémati, M., 2017. Kinetic study and modelling of char combustion in TGA in isothermal conditions. Fuel. https://doi.org/10.1016/j.fuel.2017.04.134

Radovic, L.R., Silva-Villalobos, A.F., Silva-Tapia, A.B., Vallejos-Burgos, F., 2011. On the mechanism of nascent site deactivation in graphene. Carbon N. Y. 49, 3471–3487. https://doi.org/10.1016/j.carbon.2011.04.046

William C. Hinds, 1999. Aerosol technology properties behavior and measurement of airborne particles, 2nd ed, A Wiley-Interscience Publication John Wiley & Sons, inc. https://doi.org/10.1533/9781845695750.frontmatter